LMSC-D877499

INVESTIGATION OF A PARA-ORTHO HYDROGEN REACTOR FOR APPLICATION TO SPACECRAFT SENSOR COOLING

FINAL REPORT
JANUARY 1983

by T.C.Nast

FOR NASA GODDARD SPACE FLIGHT CENTER
CONTRACT NAS 5-25792
Dr. Allan Sherman, Technical Officer

Lockheed

PALO ALTO RESEARCH LABORATORIES

LOCKHEED MISSILES & SPACE COMPANY, INC. • A SUBSIDIARY OF LOCKHEED CORPORATION
PALO ALTO, CALIFORNIA

INVESTIGATION OF A PARA-ORTHO HYDROGEN REACTOR FOR APPLICATION TO SPACECRAFT SENSOR COOLING

FINAL REPORT

JANUARY 1983

by T. C. Nast

FOR NASA GODDARD SPACE FLIGHT CENTER
CONTRACT NAS 5-25792

Dr. Allan Sherman, Technical Officer

Applied Materials and Technology Laboratory
Lockheed Missiles & Space Company, Inc.
3251 Hanover Street
Palo Alto, California 94304

FOREWORD

The Lockheed Palo Alto Research Laboratory is submitting this final report in fulfillment of the requirements of Contract NAS 5-25792. Mr. T. C. Nast was Lockheed Project Manager, and Dr. Allan Sherman was the NASA-Goddard Space Flight Center Technical Officer. Mr. G. Bell did the initial work on the design of the test apparatus. Mr. R. Grayson performed the literature search and trade studies on the reactor. Mr. L. Naes performed a detailed thermal analysis of the reactor assembly, and Dr. I. Hsu assisted in the testing and data reduction.

CONTENTS

ILLUSTRATIONS

TABLES

Section 1
INTRODUCTION

The utilization of solid hydrogen in space for sensor and instrument cooling is a very efficient technique for long-term cooling or for cooling at high heat rates. The solid hydrogen can provide temperatures as low as 7-8 K to instruments. Vapor cooling can be utilized to reduce parasitic heat inputs to the 7-8 K stage and can be effective in providing intermediate cooling for instrument components operating at higher temperatures. The use of solid hydrogen in place of helium may lead to weight reductions as large as a factor of ten and an attendent reduction in system volume.

Hydrogen exists in two different molecular states: the para form in which the protons have opposing spins, and the more energetic ortho form which has unidirectional spins. At room temperature, normal hydrogen consists of approximately 25 percent para and 75 percent ortho, while at the normal boiling point temperature of 20.4 K and lower, the mixture is greater than 99 percent para. The endothermic conversion from 99 percent para to the equilibrium composition, which is temperature dependent, is an extremely slow reaction requiring hundreds of hours. Use of an appropriate catalyst can reduce the reaction time to fractions of a second. It is, therefore, possible to develop a catalytic reactor which can be located in the hydrogen vent line of a dewar and will use the endothermicity of the para to ortho conversion to enhance instrument cooling with hydrogen.

This report presents the results of an investigation of a catalytic reactor for use with a solid hydrogen cooling system. Trade studies were performed on several configurations of reactor to meet the requirements of high reactor efficiency with low pressure drop. Results for the selected reactor design are presented for both liquid hydrogen systems operating at near atmospheric pressure and the solid hydrogen cooler operating as low as 1 torr.

Section 2
DESIGN AND ANALYSIS

2.1 APPLICATION TO INSTRUMENT COOLING

A class of infrared instruments (Refs. 1 and 2) requires detector cooling to 10-13 K and also incorporates a cooled baffle which must operate in the 80-150 K temperature range to limit the background photon flux. The solid hydrogen provides the focal plane cooling, while the baffle is cooled with vapor from the sublimation of H_2. A substantial increase in baffle cooling can be achieved by incorporation of the endothermic catalytic converter at the baffle. Fig. 2-1 shows the heat of conversion in the reactor as a function of reactor temperature. As the curve shows, the maximum heat of conversion occurs at 105 K.

The following describes the comparative benefits associated with various reactor employments. For comparison with vapor cooling only it is assumed that an optics module is cooled to 30 K with H_2 vapor.

Figures 2-2, 2-3, and 2-4 are enthalpy-temperature plots representing the overall thermodynamics of the catalytic conversion system. Figure 2-2 shows lines of 100 percent para and equilibrium compositions. Figures 2-3 and 2-4 show an equilibrium composition line and percent para lines from 0 to 100 percent in increments of 10 percent.

Two operating process alternatives are of interest: an adiabatic catalytic converter and an isothermal reactor. Both options use heat exchange from the baffle to warm the hydrogen gas from 30 K (optics temperature) and then to 100 K (baffle temperature) (points (1) to (2) on the process diagrams). At this point, because of the slow rates of equilibration, the gas stream is still almost completely in the form of para-hydrogen. In the adiabatic reactor, the catalyst causes the gas to quickly reach near 100 percent of its

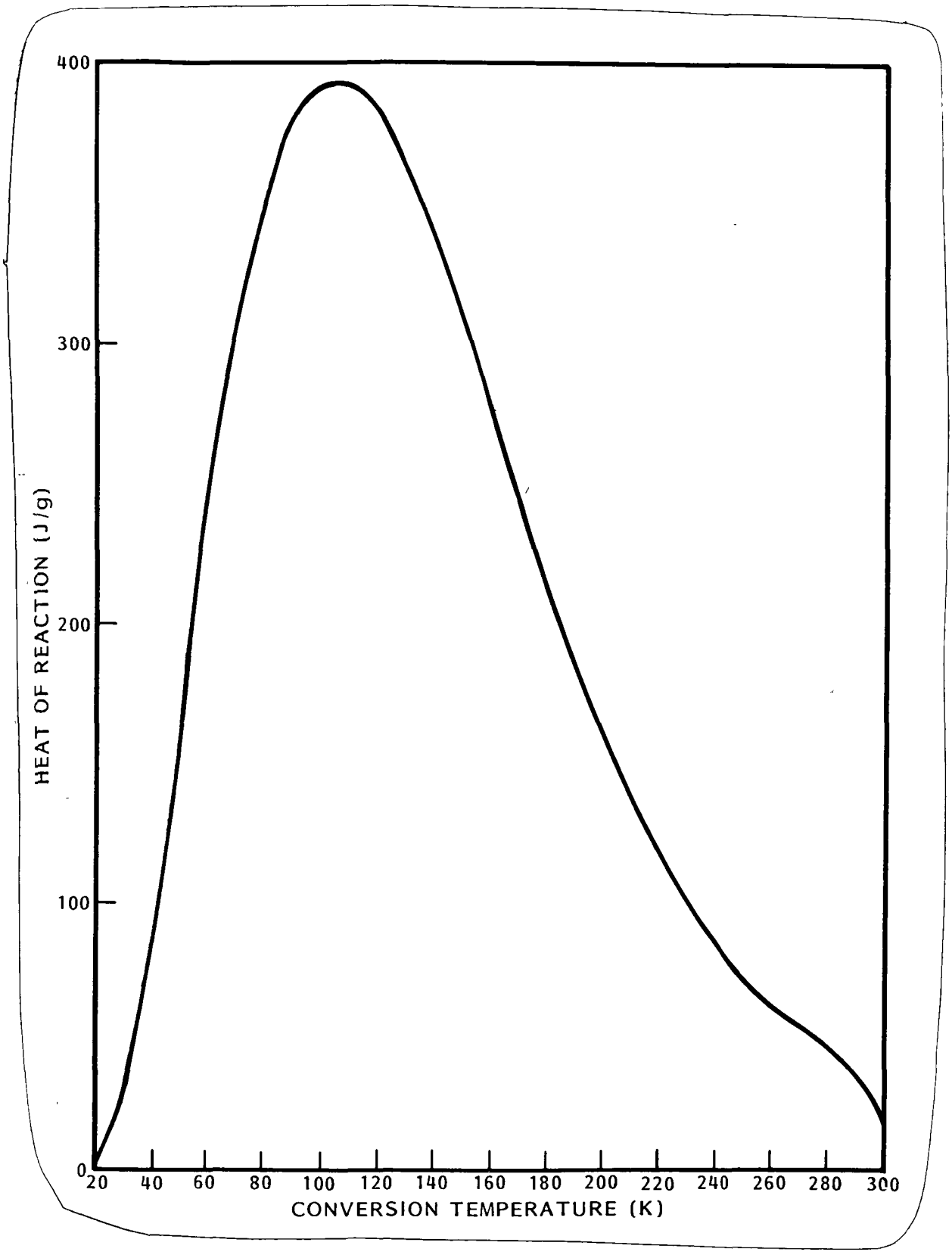

Fig. 2-1 Para-Ortho Heat of Conversion Versus Conversion Temperature

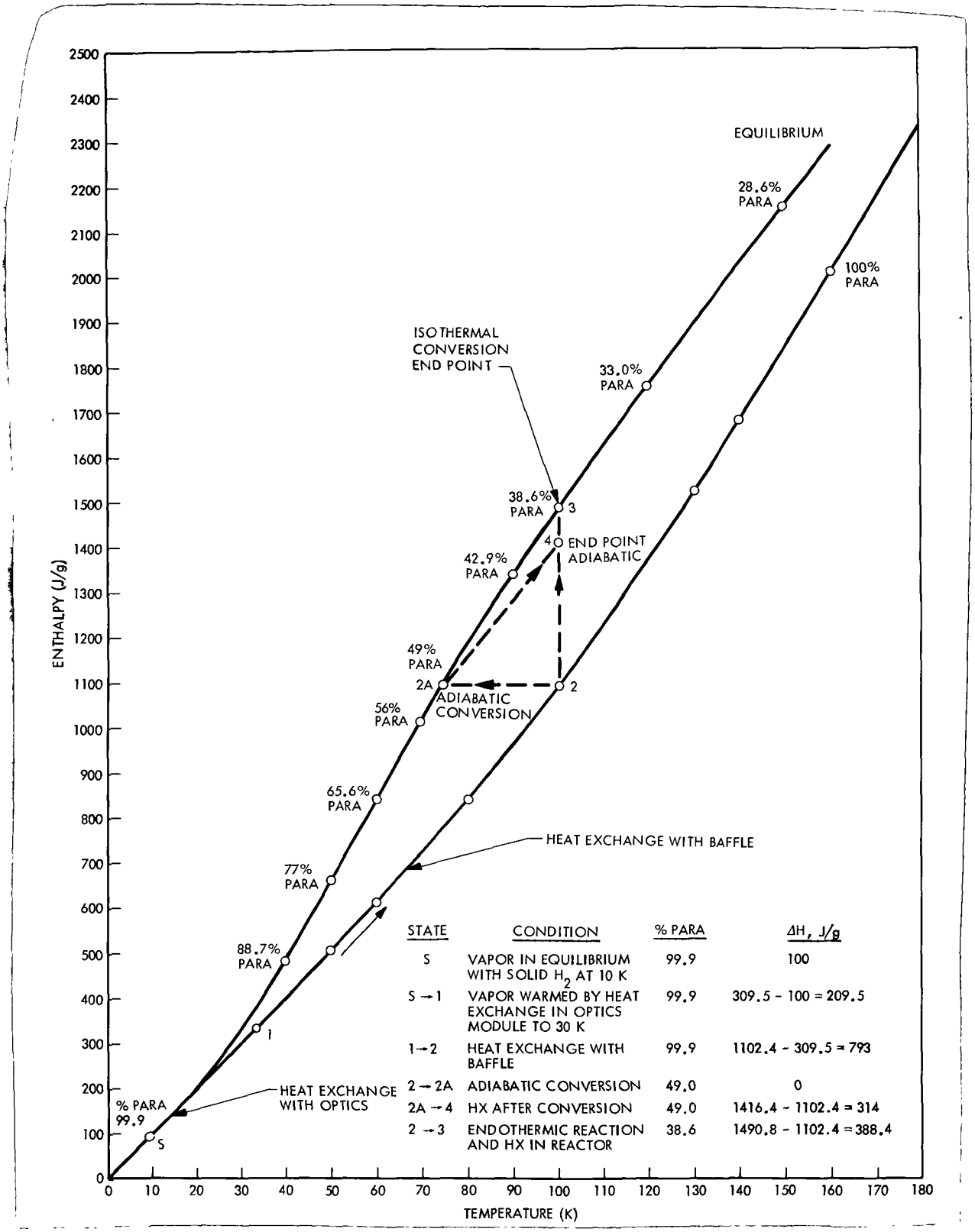

Fig. 2-2 Overall System Process Diagram

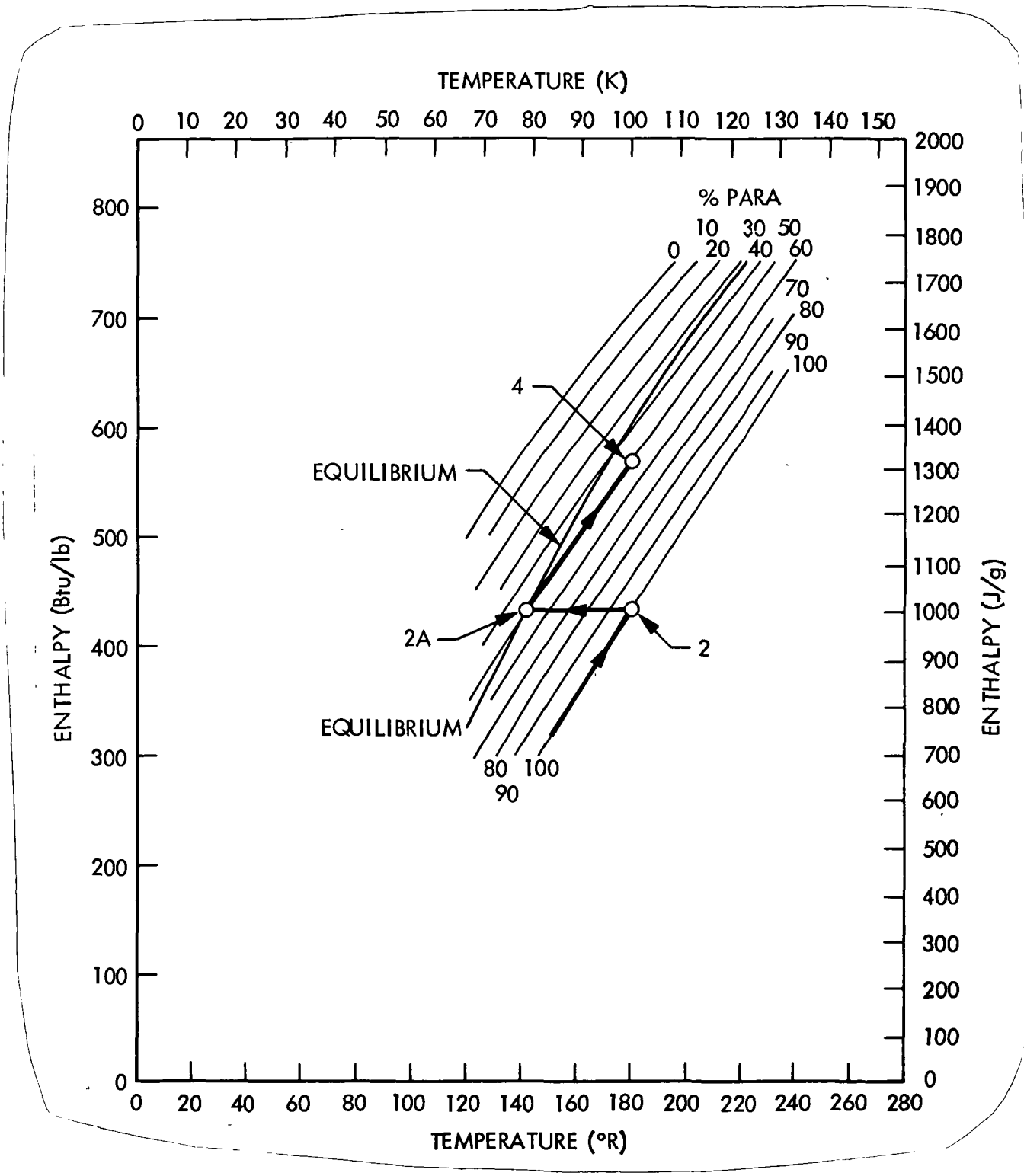

Fig. 2-3 Adiabatic Process Diagram

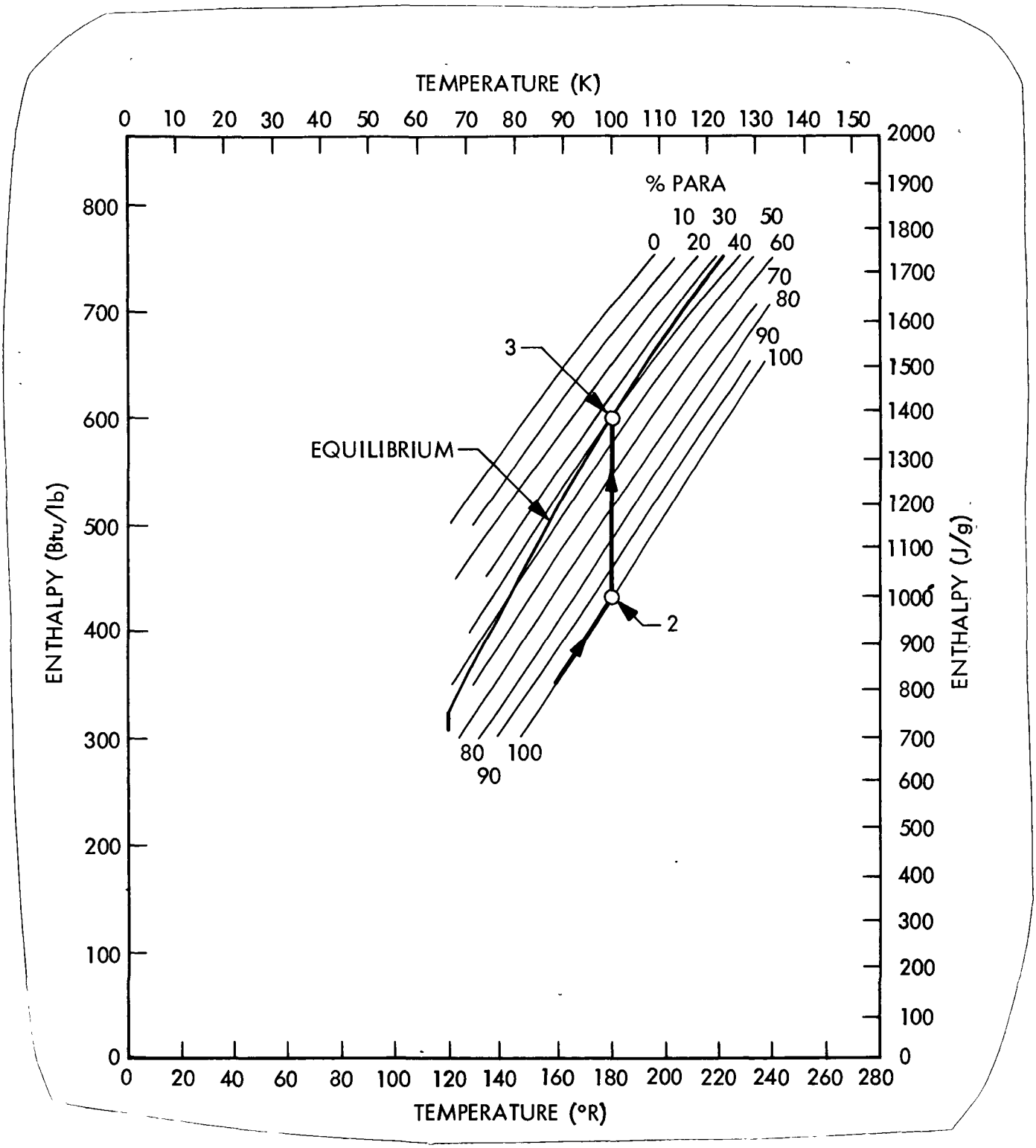

Fig. 2-4 Isothermal Process Diagram

equilibrium composition along a line of constant enthalpy. Since the para to ortho conversion is an endothermic process, energy is removed from the gas, causing the temperature to drop to about 79 K. The equilibrium composition at this point ((2a) on the process diagrams) is 49 percent para. Because of the very slow uncatalyzed reaction rates in the exit line, the gas is warmed by the baffle along a line of constant composition (49 percent para) to a final temperature of 100 K (point (4) on the process diagrams), a process which contributes an additional 314 J/g cooling capacity to the uncatalyzed case (1107 J/g versus 793 J/g, respectively). Ten watts of cooling may therefore be attained by the adiabatic reactor with a hydrogen mass flow rate of 0.00903 g/s. With a flow rate equal to 0.01 g/s, 11.1 W may be extracted from a 100 K baffle.

The isothermal reactor utilizes heat from the baffle to maintain a constant gas temperature during a continuous conversion to the equilibrium composition of 38.6 percent para at 100 K (point (3) on the process diagrams). There is no further heat exchange in the exit line.

The enthalpy values for the various processes and a comparison of the heat absorbed in the various processes are shown in Tables 2-1 and 2-2.

The test reactor will be designed for adiabatic operation, due to the difficulties inherent in ensuring adequate heat transfer in the small catalyst space as is required by the isothermal condition. However, because of heat leaks from the test apparatus to the reactor, actual operation will be between the adiabatic and isothermal conditions.

2.2 CATALYST SELECTION AND REACTIVITY

At low temperatures, the spontaneous conversion of para-H_2 to the equilibrium composition is very slow and is attributed to magnetic interreactions between the ortho molecules. The kinetics follow a standard bimolecular rate law of $-dx/dt = Kx^2$, with an uncatalyzed rate constant

Table 2-1 STATE POINT ENTHALPIES

State/Process	H(J/g)	ΔH(J/g)	Description
1	309.5		30 K gas from optics
2	1102.4		100 K gas from baffle
1→ 2		792.9	Cooling of baffle without catalytic converter 78.9 K, 49 percent para
2	1102.4		
2→ 2A		0	Adiabatic conversion 100 K, 38.6 percent para
3	1490.8		
2→ 3		388.4	Isothermal conversion 100 K, 49 percent para
4	1416.4		
2A→ 4		314.0	Heating of state 2A gas to final temperature

Table 2-2 COMPARISON OF HEAT ABSORPTION BY VARIOUS PROCESSES

Process	ΔH, J/g
Heat absorption by vapor from 30 K to 100 K	793
Heat absorption with isothermal reactor at 100 K	388
Heat absorption with adiabatic converter	314

K = 0.114 (Ref. 3), and where x represents the concentration of ortho or para H_2. The equilibrium composition of H_2 versus temperature is shown in Figure 2-5.

An extensive literature search yielded data on activities of various catalysts including metal films, metal hydride gels, and metals supported by alumina, silica, oxides, or zeolites. In terms of a kinetic rate parameter such as Km

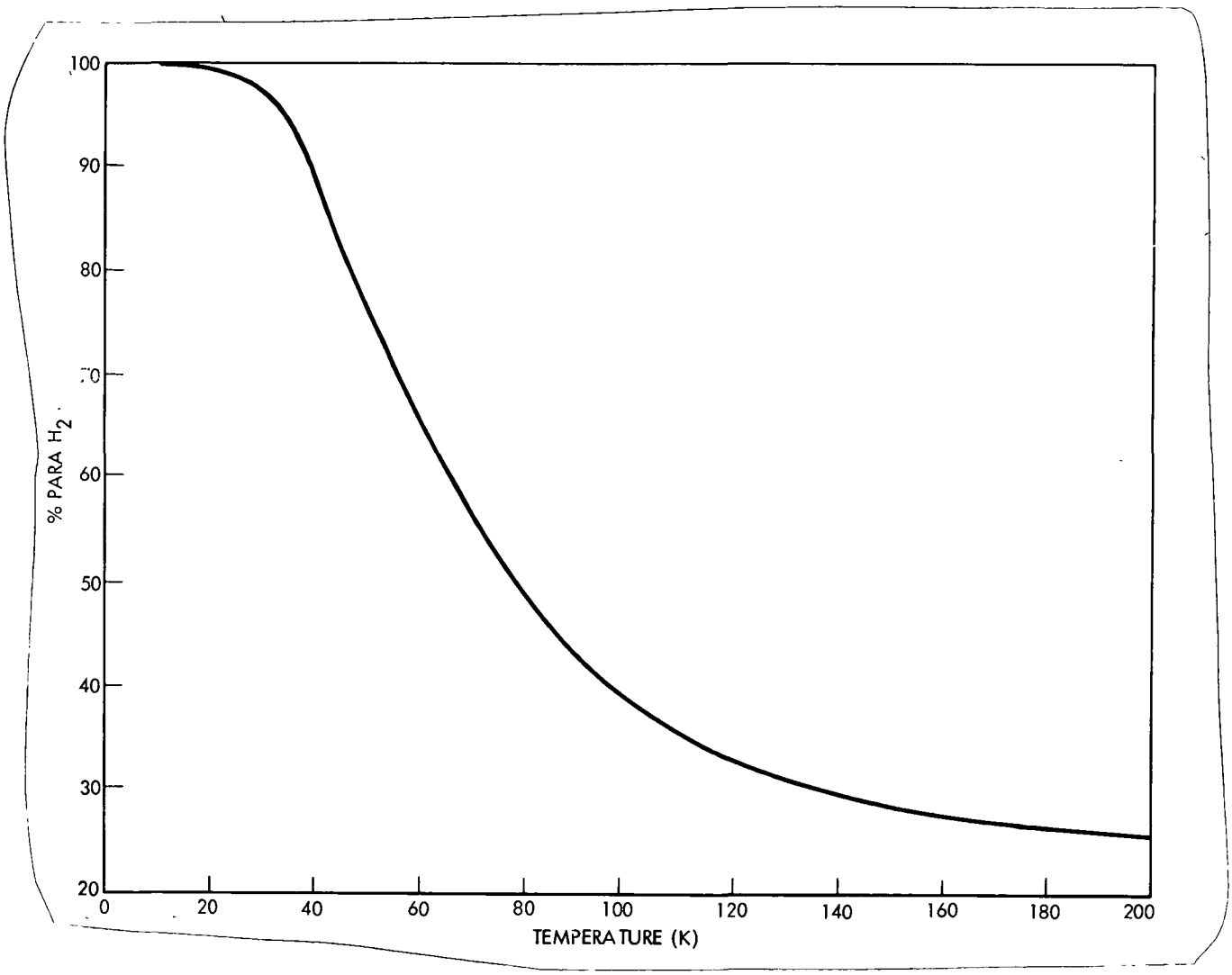

Fig. 2-5 Equilibrium Composition for Hydrogen

(molecules H_2 converted per second per mg catalyst), the most active catalysts consist of Ni, Cu, or Fe films supported by alumina or silica. Most researchers subscribe to a form of the Wigner theory of catalyst activity whereby absolute conversion rates are proportional to the square of the magnetic moment of the metal ion.

The physical mechanism of the conversion is believed to involve adsorption of the H_2 molecules on paramagnetic sites, with the overall kinetics generally following a first order Arrhenius rate law ($K_m = B_m \exp(-E/RT)$), where K_m is the catalyst specific reaction rate; B_m is the pre-exponential factor; E is the activation energy in cal/mole; and R is the specific gas constant. In addition to this mechanism, various chemical mechanisms have also been proposed. Whereas in the paramagnetic mechanism the adsorbed pH_2 molecule is magnetically switched to oH_2, the chemical mechanisms involve the splitting of the pH_2 molecule into two H atoms, each on an uncovered surface metal site of low binding energy, and then the recombination to oH_2. These are forms of the Bonhoeffer-Farkas (Ref. 4) mechanism which has no diffusion retardation since the activity is due to the catalytic surface. The chemical mechanisms are also approximately first order reversible Arrhenius reactions. Because of the nature of the conversion mechanism, the para to ortho conversion is the kinetically reversible reaction to ortho to para conversion.

Table 2-3 lists various catalysts, experimental temperatures, pressures, and relative activities found in the literature for the primary pressure range of interest (1-10 torr). In formulating a common basis of units for K_m, all catalysts were assumed to have an active surface area of 40 cm^2/mg, which is an approximate value obtained from the literature. Also shown are the values of β, which is the ratio of grams of catalyst to grams per second of hydrogen flow. This parameter is commonly used in reactor design.

Table 2-4 presents data which could not be converted to the common K_m basis. It gives an indication of the relatively high activities of the Ni/Al_2O_3 catalysts. However, note that the order of the most active

Table 2-3 ACTIVITIES OF VARIOUS CATALYSTS ((Ref. 12))

Catalyst	T(K)	P(torr)	$\beta(\frac{g\ catalyst}{gH_{2/s}})$	$K_m(\frac{molecules}{mg/s})$	Author
Zeolite	77-90	7	$2.1x10^6$	$1.4x10^{14}$	(Ref. 5) Rudham, 1975
Pd^{+2}/Zeolite	"	"	$4.8x10^5$	$6,2x10^{14}$	" "
Mole Sieve	"	"	$8.5x10^4$	$3.5x10^{15}$	(Ref. 6) Brown,1970
Nd^{+3}/Mole Sieve	"	"	$4.3x10^4$	$6.9x10^{15}$	" "
Mn^{+2}/Zeolite	"	"	$3.1x10^4$	$9.6x10^{15}$	(Ref. 5) Rudham, 1975
Co^{+2}/Zeolite	"	"	$2.5x10^4$	$1.2x10^{16}$	" "
Ni^{+2}/Zeolite	"	"	$2.3x10^4$	$1.3x10^{16}$	" "
Cu^{+2}/Zeolite	"	"	$2.0x10^4$	$1.5x10^{16}$	" "
Rhenium Powder	77-368	10-180	$7.5x10^3$	$4.0x10^{16}$	(Ref. 7) Kubicka, 1971
Dy_2O_3	-	7.6	$1.0x10^3$	$3.0x10^{17}$	(Ref. 8) Eley, 1974
Ni; NiH_2 Films	170-195	2	$1.0x10^3$	$3.0x10^{17}$	(Ref. 9) Frankiewicz, 1975
Nd_2O_3	-	7.6	$6.4x10^2$	$4.7x10^{17}$	(Ref. 8) Eley, 1974
Fe	90	1.2	$5.7x10^2$	$5.2x10^{17}$	(Ref. 10) Eley, 1963
Fe	273	1.2	$5.2x10^2$	$5.7x10^1$	" "
Ni	"	1.2	$4.5x10^2$	$6.7x10^{17}$	" "
Co	"	1.2	$4.0x10^2$	$7.4x10^{17}$	" "
Fe_2O_3 gel		$2.07x10^5$Pa	$8.8x10^1$	$3.4x10^{18}$	(Ref. 11) Weitzel
$NiO{\cdot}2.5\ SiO_2$ gel		$2.07x10^6 \sim 1.03x10^7$Pa	$3.6x10^1$	$8.4x10^{18}$	(Ref. 12) Singleton, 1967

catalysts (Ni/Al_2O_3 and hydrous ferric oxide gel) vary according to each author and method of preparation.

Table 2-5 presents a summary of test data on a high surface area Ni on silicate catalyst (APACHI-1) at pressures in the range of $3.52 \times 10^5 \sim 1.03 \times 10^7$Pa. The data are summarized in Fig. 2-6 in terms of β versus pressure. Only β values for near complete conversion ($\geq$95 percent) are shown.

The available data on the catalysts indicate the APACHI-1 is among the most active if not the most active catalyst available. In addition it is commercially available, whereas most of the others are available in experimental batches or not at all. Based on these considerations, APACHI-1 was selected for reactor studies. Unfortunately, data on the APACHI-1 at low pressure is not available. Therefore an extrapolation to the operating pressure of ~ 2 torr is required.

A minimum value of β of 1000 based on a study of the data was selected for design. This value is shown in Fig. 2-6.

2.3 DESIGN TRADES

Having selected a value of β of 1000 g catalyst per g H_2/s flow rate, which our extrapolation of available data indicates will yield complete conversion, the primary problem is minimizing the pressure drop in the reactor. The catalyst volume required is based on a catalyst density of 0.45 g/cm^3.

Pressure drop through the catalyst bed was calculated using the Ergun relationship for pressure drop through packed beds with negligible static head and for particles of similar size and shape. The relationship may be expressed as:

Table 2-4 ACTIVITIES OF SOME OTHER CATALYSTS

Catalyst Sample	T	Density (g/cm^3)	Wt (g)	Pressure ($x10^6 Pa$)	Act. Ener. (E) kcal/mole	K	Relative Activity
19% Cr_2O_3/Al_2O_3	77 K	1.34	9.30	2.86 0.79 0.45	0.99 0.99 0.99	$0.099x10^{-4}$ $0.076x10^{-4}$ $0.060x10^{-4}$	1.0
0.5% CuO/Al_2O_3		1.26	3.86	2.86 0.79	0.97 0.98	$0.33x10^{-4}$ $0.27x10^{-4}$	3.3
0.5% NiO/Al_2O_3		1.43	3.66	2.86 0.79	0.95 0.96	$0.51x10^{-4}$ $0.34x10^{-4}$	5.2
0.5% Cu/Al_2O_3		1.26	3.86	2.86 0.79	- -	0 0	0
0.5% $Ni(A)/Al_2O_3$		1.43	3.66	2.86 0.79 0.45	0.77 0.81 0.85	$3.0x10^{-4}$ $2.2x10^{-4}$ $1.7x10^{-4}$	30
Ferric Oxide Gel (Weitzel)							4.0
Most Active 0.5% $Ni(B)/Al_2O_3$ on a Wt.basis		1.33	3.21	2.86 0.45	0.70 0.81	$5.2x10^{-4}$ $2.7x10^{-4}$	53
0.5% Mn_2O_2/Al_2O_3		1.28	3.38	2.86 0.79	0.94 0.95	$0.76x10^{-4}$ $0.63x10^{-4}$	7.7
0.5% Tb_2O_3/Al_2O_3		1.69	4.70	2.86 0.79	0.93 0.94	$0.41x10^{-4}$ $0.32x10^{-4}$	4.1
0.5% Pd/Al_2O_3		1.41	4.11	2.86 0.79	- -	0 0	0
5.0% $Ni(I)Al_2O_3$		1.84	3.84	2.86 0.79	0.85 0.86	$0.84x10^{-4}$ $0.69x10^{-4}$	8.5
5.0% $Ni(X)\ Al_2O_3$		1.91	2.55	2.86 0.79	0.42 0.45	$8.9x10^{-4}$ $5.7x10^{-4}$	90
0.5% TbO_2/ZrO_2		3.63	6.58	2.86 0.79 0.45	0.96 0.97 0.98	$0.20x10^{-4}$ $0.17x10^{-4}$ $0.11x10^{-4}$	2.0

Table 2-5 APACHI-1 CATALYST ACTIVITY

Point	Tin(K)	P(Pa)	M(g/s)	Dp(mesh)	$\beta(\frac{g\ catalyst}{gH_{2/s}})$	% equilibrium conversion
1	86.7	$3.50x10^5$	.668	16-25	104.	94.3
2	97.8	$3.72x10^5$	.643	30-40	61.8	100
3	76.7	$3.72x10^5$	.655	30-40	80.8	98.5
4	110	$3.72x10^5$	.630	30-40	84.	99.9
5	97.2	$3.72x10^5$	.630	30-40	82.4	99.8
6	86.7	$3.72x10^5$	.643	30-40	82.4	96.5
7	86.7	$3.72x10^5$	.428	30-40	124.	98.8
8	70.6	$3.72x10^5$	.643	30-40	61.8	99.2
9	132.8	$3.65x10^5$	.668	16-25	104.	96.0
10	132.8	$3.50x10^5$	.435	16-25	160.	99.7
11a	119.4	$3.72x10^5$	.605	30-40	110.	99.7
11b	119.4	$3.72x10^5$	.605	30-40	87.7	99.0
12	90.	$3.72x10^5$	.643	30-40	82.4	100.
13	67.2	$3.72x10^5$	.655	30-40	80.8	100.
14	56.1	$3.72x10^5$	.655	30-40	80.8	99.5
15	147.8	$3.65x10^5$	.504	50-80	117.	98.3
16	110.	$3.65x10^5$	.580	50-80	81.6	99.6
17a	88.9	$3.65x10^5$	.605	50-80	78.	100.
17b	88.9	$3.65x10^5$	.605	50-80	74.9	100.
18	79.4	$3.65x10^5$	.605	50-80	78.	100.
19	67.2	$3.65x10^5$	.630	50-80	74.9	100.
20	56.7	$3.65x10^5$	.643	50-80	73.5	100.
21	133.9	$3.78x10^5$	.643	16-25	102.	99.5
22	88.9	$3.72x10^5$	.491	80-140	83.9	93.9
23	122.8	$3.78x10^5$	.416	80-140	99.	64.7
24	111.1	$3.72x10^5$	.454	80-140	90.8	81.5
25	100.	$3.72x10^5$	.491	80-140	83.9	90.
26	66.7	$3.72x10^5$	.567	80-140	52.5	96.4
27	56.1	$3.72x10^5$	.580	80-140	51.3	96.4
28	147.2	$3.72x10^5$	.340	80-140	121.	26.7

Table 2-5 APACHI-1 CATALYST ACTIVITY (Continued)

Point	Tin(K)	P(Pa)	M(g/s)	Dp(mesh)	$\beta(\frac{g\ catalyst}{gH_{2/s}})$	% equilibrium conversion
29	144.4	$3.72x10^5$	.340	80-140	121.	26.7
30	141.7	$3.72x10^5$	.353	80-140	117.	32.1
31	138.9	$3.72x10^5$	.325	80-140	113.	36.6
32	76.1	$3.72x10^5$	.567	80-140	53.7	99.3
33	100.	$6.93x10^6$	.630	50-80	23.6	92.7
34	99.4	$7.17x10^6$	1.273	50-80	11.8	68.9
35	143.9	$1.05x10^7$	.630	50-80	23.6	77.7
36	121.7	$1.06x10^7$	.617	50-80	24.2	87.8
37	100.	$1.05x10^7$	.617	50-80	24.2	94.8
38	78.9	$1.04x10^7$	.617	50-80	24.2	96.0
39	99.4	$1.05x10^7$	1.273	50-80	11.8	70.5
40	100.6	$7.01x10^6$	.592	50-80	25.1	91.5
41	100.	$3.46x10^6$	.592	50-80	25.1	92.5
42	122.2	$6.87x10^6$	.617	50-80	24.2	83.5
43	111.1	$1.05x10^7$	.630	50-80	23.6	89.0
44	88.9	$1.04x10^7$	.630	50-80	23.6	94.8
45	77.8	$6.96x10^6$	.592	50-80	25.1	90.8
46	144.4	$1.05x10^7$	.617	30-40	26.8	89.4
47	122.2	$1.05x10^7$	.630	30-40	26.2	93.0
48	100.	$1.05x10^7$	.617	30-40	26.8	96.0
49	100.	$1.04x10^7$	1.285	30-40	12.9	75.0
50	122.2	$6.94x10^6$	.617	30-40	26.8	92.5
51	99.4	$7.09x10^6$	.617	30-40	26.8	94.5
52	100.	$7.04x10^6$	1.273	30-40	13.0	75.0
53	77.2	$7.05x10^6$	.617	30-40	26.8	97.6
54	100.	$3.53x10^6$	.617	30-40	26.8	96.1
55	78.3	$1.03x10^7$	.617	30-40	26.8	95.8
56	98.9	$1.04x10^7$	.617	16-25	27.5	94.0

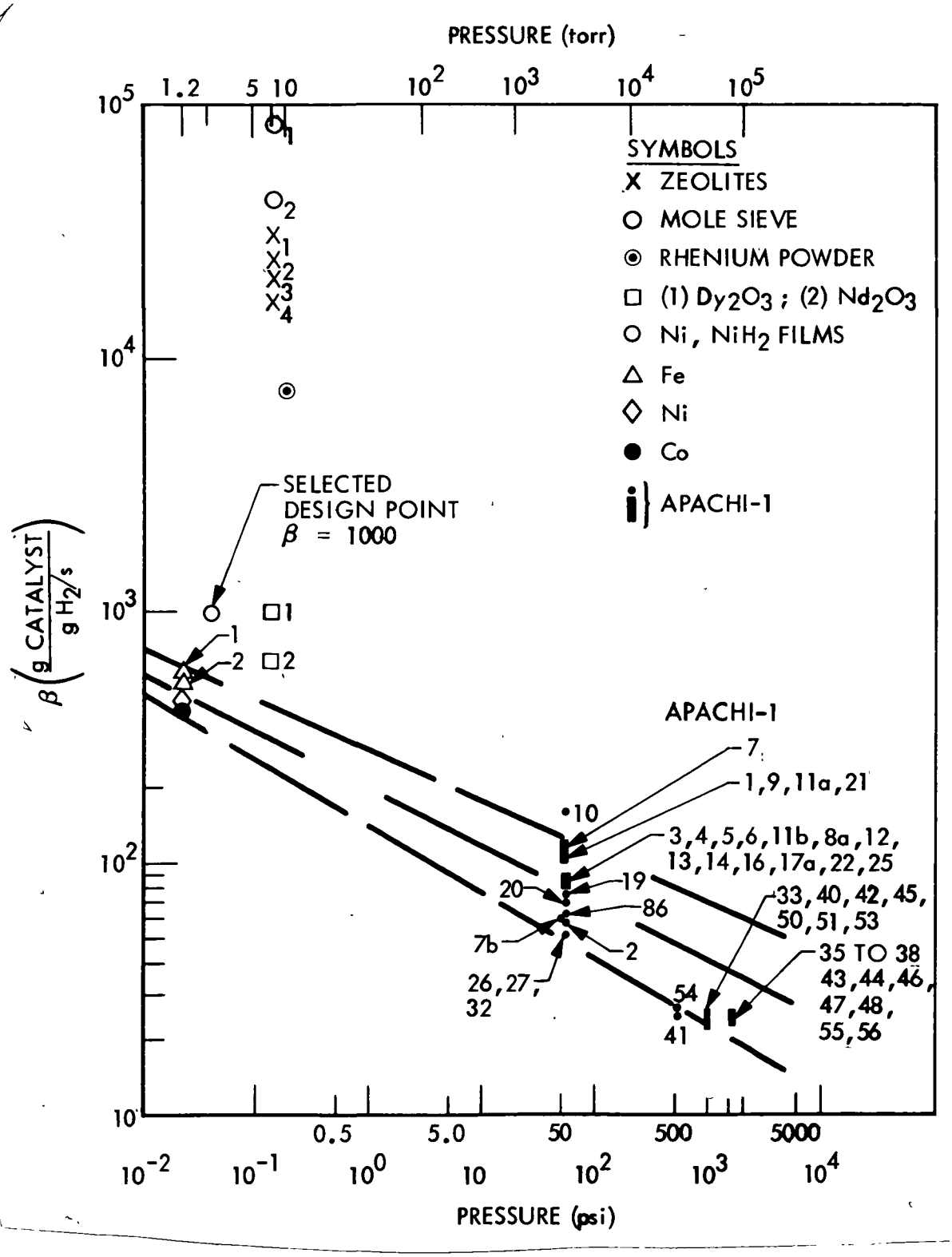

Fig. 2-6 Catalyst Activities Versus Pressure - Experimental Data

$$\frac{\Delta P}{L} = \frac{150(1-\epsilon)^2}{\epsilon^3}\frac{\mu U_m}{D_p^2 g_c} + \frac{1.75(1-\epsilon)G\,U_m}{\epsilon^3 D_p g_c}$$

where

G = ρU mass flowrate of fluid in tube (lb_m/ft^2 s)
U_m = superficial fluid velocity at average pressure (ft/s)
D_p = particle diameter (ft)
ϵ = fractional void volume in bed
μ = fluid viscosity at average temperature and pressure (lb_m/ft s)
$\frac{\Delta P}{L}$ = pressure drop per unit length ($lb_f/ft^2/ft$)
U = superficial fluid velocity based on empty column cross section (ft/s)

Since $G = \rho U = \dot{m}/A$, $g_c = 32.2$ ft lb_m/lb_f s^2, and ϵ was assumed equal to 0.45 (a value obtained from the literature), the Ergun equation may be simplified to:

$$\frac{\Delta P}{L} = \left[\frac{82.5\mu}{D_p} + 1.75G\right] \frac{0.1874G}{D_p\rho}$$

The first term is the viscous contribution, while the second part is the energy term. The pressure drop is dependent upon the size and shape of the catalyst particles and not upon the material. Therefore, this equation is valid for any catalyst.

Two design options were considered: a cylindrical and a radial flow reactor. Because of the low pressure drop requirements for a solid H_2 cooler, the cylindrical design must be thin and have a large cross-sectional area, much like a pancake. In the radial flow reactor, gas enters through a central tube and flows radially outward through the toroidal catalyst bed and into the outer annulus, where it flows axially out of the reactor section. For an

equivalent reactor diameter and catalyst weight, the radial flow reactor has much less pressure drop than the cylindrical. The only advantage inherent in the latter lies in its relative simplicity. To achieve pressure drops about equal to those in the radial flow reactor, the cylindrical reactor must have a bed diameter of 2.5 in. This leads to a very thin bed (0.28 in.) under the constraint of a fixed $\beta = 1000$.

Figures 2-7 and 2-8 show reactor pressure drop as a function of particle mesh size, reactor length, and radial size. Each line represents a combination of particle and radial size; inner tube diameter and annulus width for the radial flow reactor and bed diameter for the cylindrical. The abscissa for the cylindrical reactor is reactor length. Fixing an appropriate length determines β for each specific bed diameter. For the radial flow reactor, the abscissa is the catalyst thickness, which together with the other two radial dimensions and the catalyst packing density determines β.

For a radial flow reactor which has an inlet tube diameter of 0.5 in., a catalyst bed radial thickness of 0.25 in., and an axial length of 2.073 in., and an outer annulus of 0.25 in., the total inside diameter is 1.5 in., with a packed catalyst weight of 10.0 g. Pressure drops through the reactor for 10, 15 and 20 mesh particles are predicted to be 0.13, 0.23, and 0.37 torr, respectively, for a mass flow rate of 0.01 g H_2/s, an inlet temperature of 100 K, and an inlet pressure of 2 torr, which is the vapor pressure of gas over solid hydrogen at about 10 K. The general configuration of the reactor designs is shown in Figs. 2-9 and 2-10.

2.4 SELECTED CONVERTER DESIGN

The final catalytic converter design is shown in Fig. 2-9. The catalyst is retained with fine mesh stainless steel screen. Threaded plugs in the end cap permit loading and unloading of the catalyst. The volume of the catalyst space is 51.5 cm^3. This design gives a β value of 2,490 s^{-1} based on a flow rate of 0.01 g/s H_2 and a measured catalyst quantity of 24.9 g. This value exceeds the estimated required value of 1000 s^{-1}.

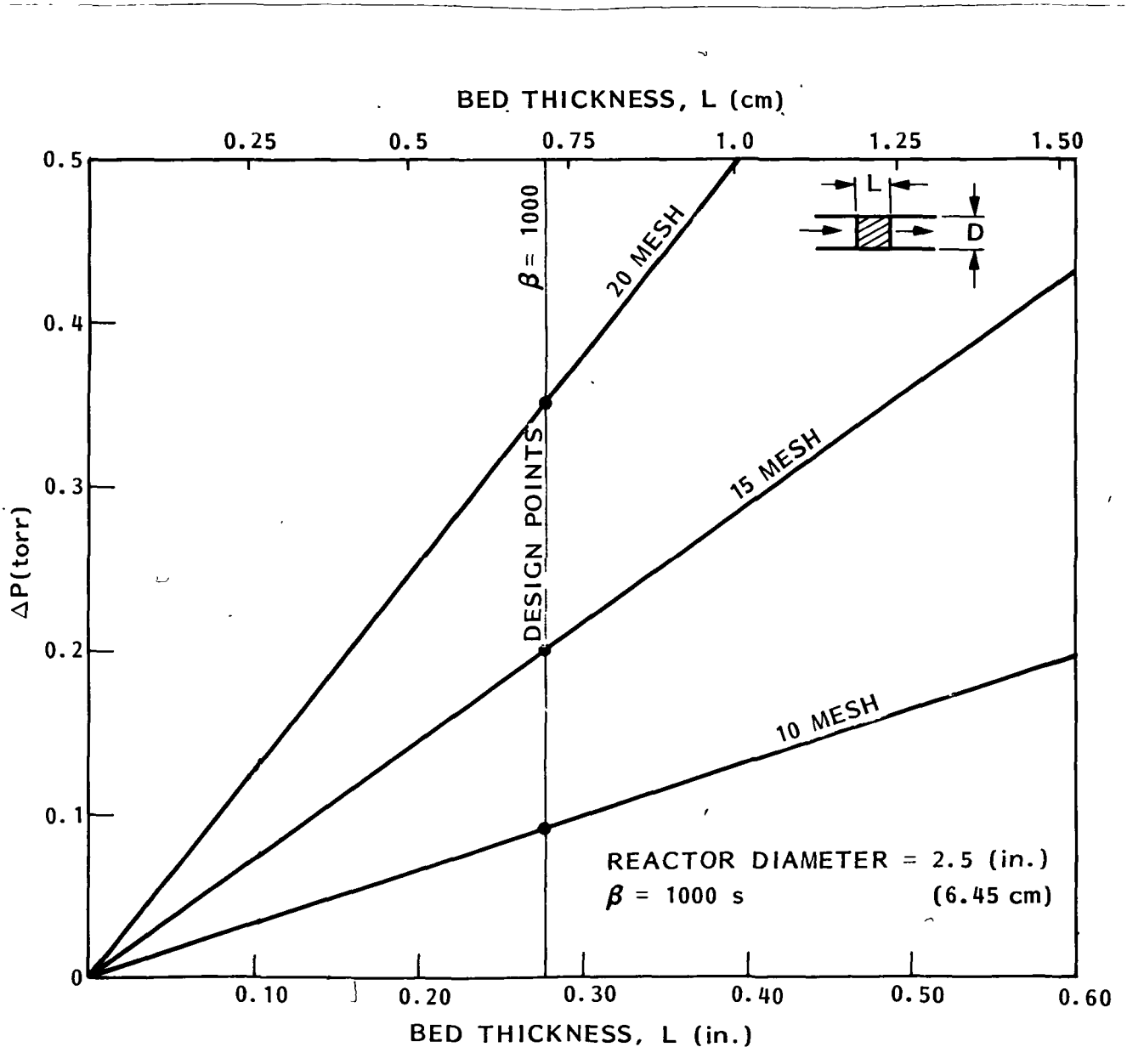

Fig. 2-7 Cylindrical Bed Reactor Pressure Drop

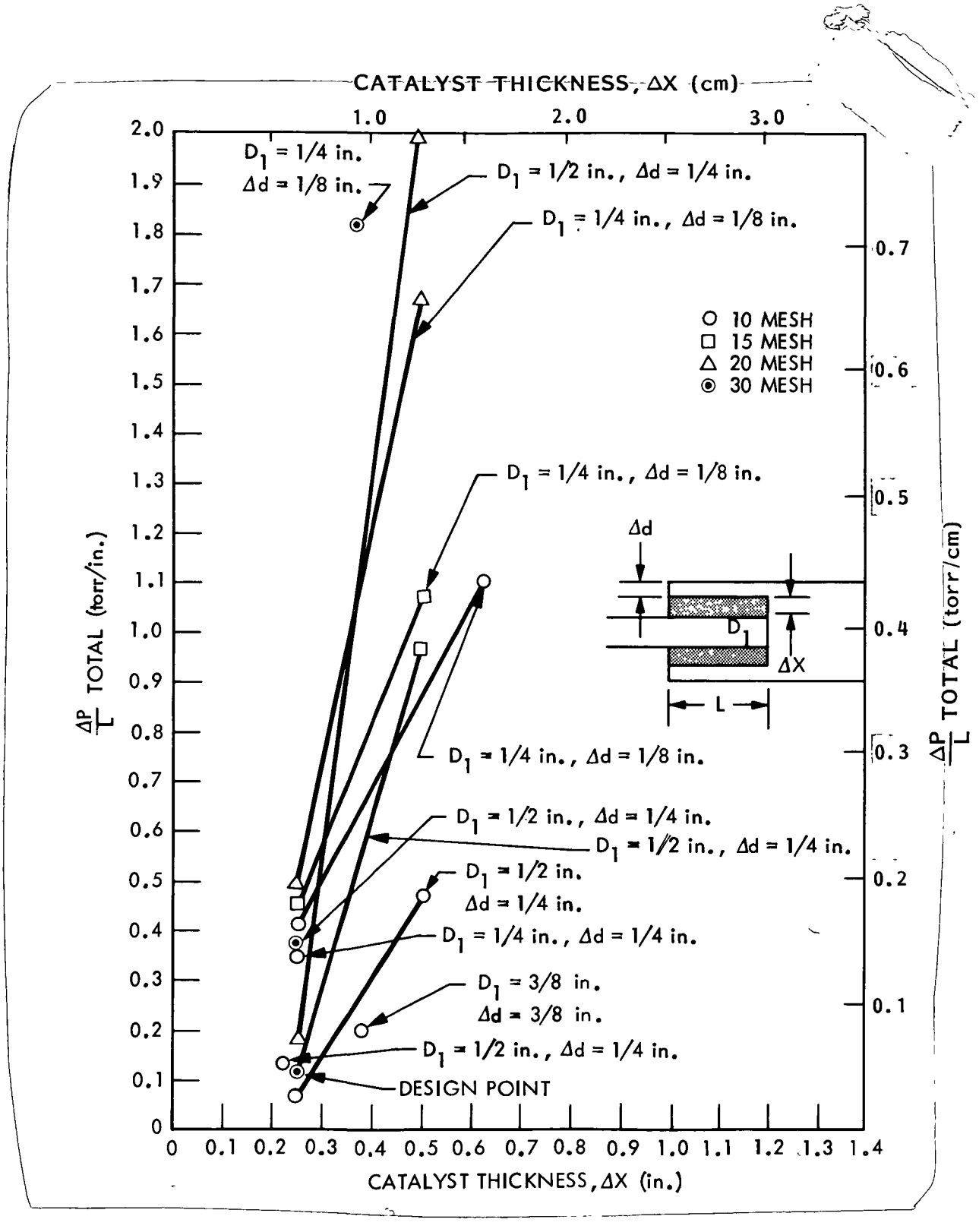

Fig. 2-8 Radial Flow Reactor Pressure Drop

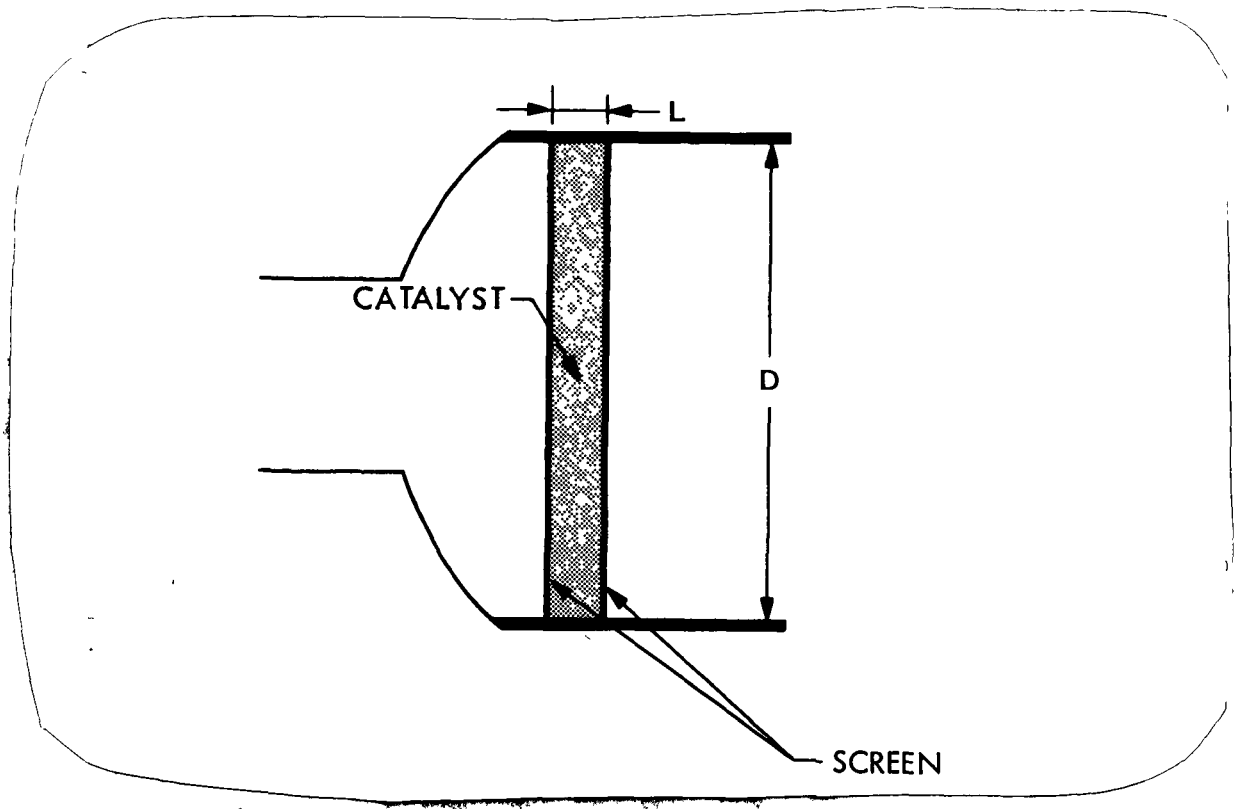

Fig. 2-9 Cylindrical Bed Reactor Configuration

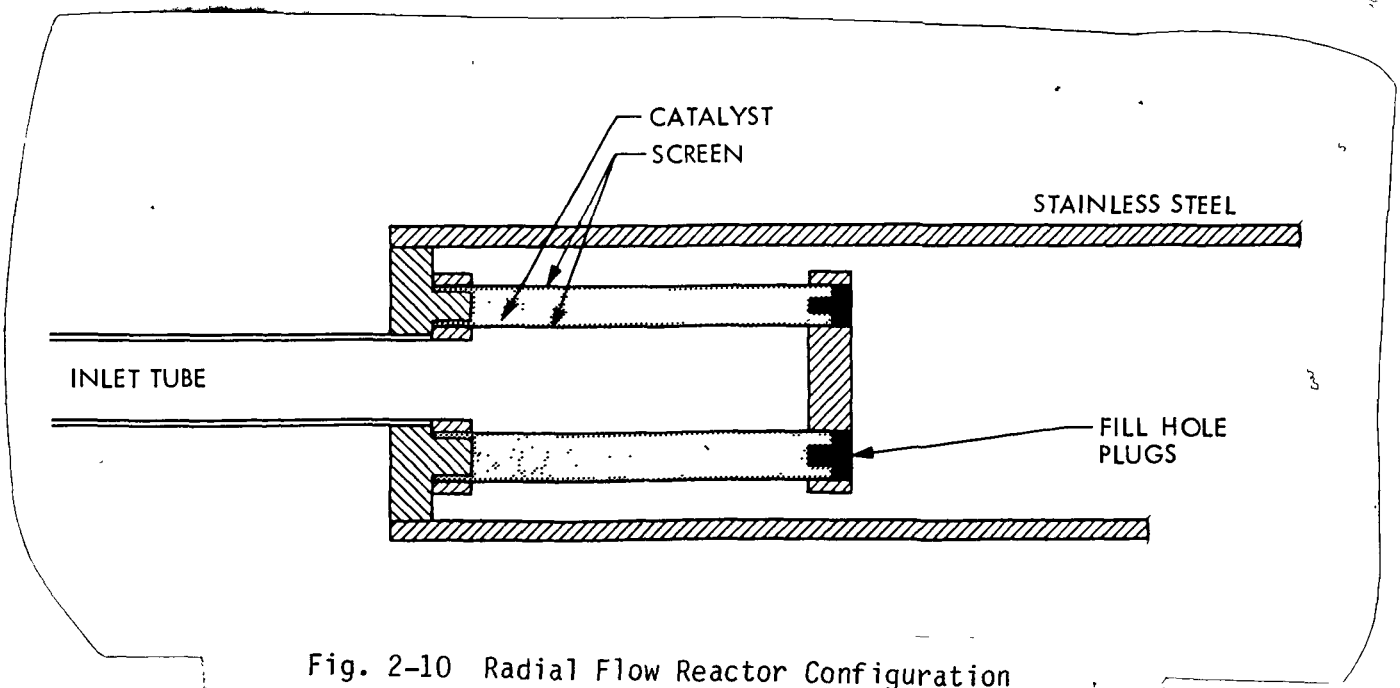

Fig. 2-10 Radial Flow Reactor Configuration

Figs. 2-12 and 2-13 show the reactor during fabrication. The outer retaining screen is visible on Fig. 2-12 as is the outer thermocouple rake for measurement of gas temperatures. Fig. 2-13 shows the outer tube of the reactor. The vacuum tight wire feed-throughs are also visible. Two pressure ports to measure inlet and outlet temperatures can also be seen. The end cap with the filling plugs is visible.

The reactor was loaded with HSC-197 (APACHI-1) catalyst available from Air Products and Chemicals, Inc. The catalyst was 30 x 50 mesh from batch no. 198CX6-2 which was tested for reactivity by Air Products. The chemical formulation is $NiSiO_4 \cdot (SiO_3)_{3.2} \cdot (H_2O)_{5.6}$. A summary of reactor characteristics is presented in Table 2-6.

Table 2-6 SUMMARY OF REACTOR CHARACTERISTICS

Catalyst Type:	HSC-197 (APACHI-1), Nickel on Silica O-P H_2 Shift (30 x 50 Mesh) Sample No. 198Cx6-2
Catalyst Quantity:	24.9 g
Overall Diameter:	2 in. (5.08 cm)
Overall Length:	5.5 in. (14.0 cm)
Catalyst Volume:	51.5 cm^3
Effective Density as Loaded:	0.484 g/cm^3

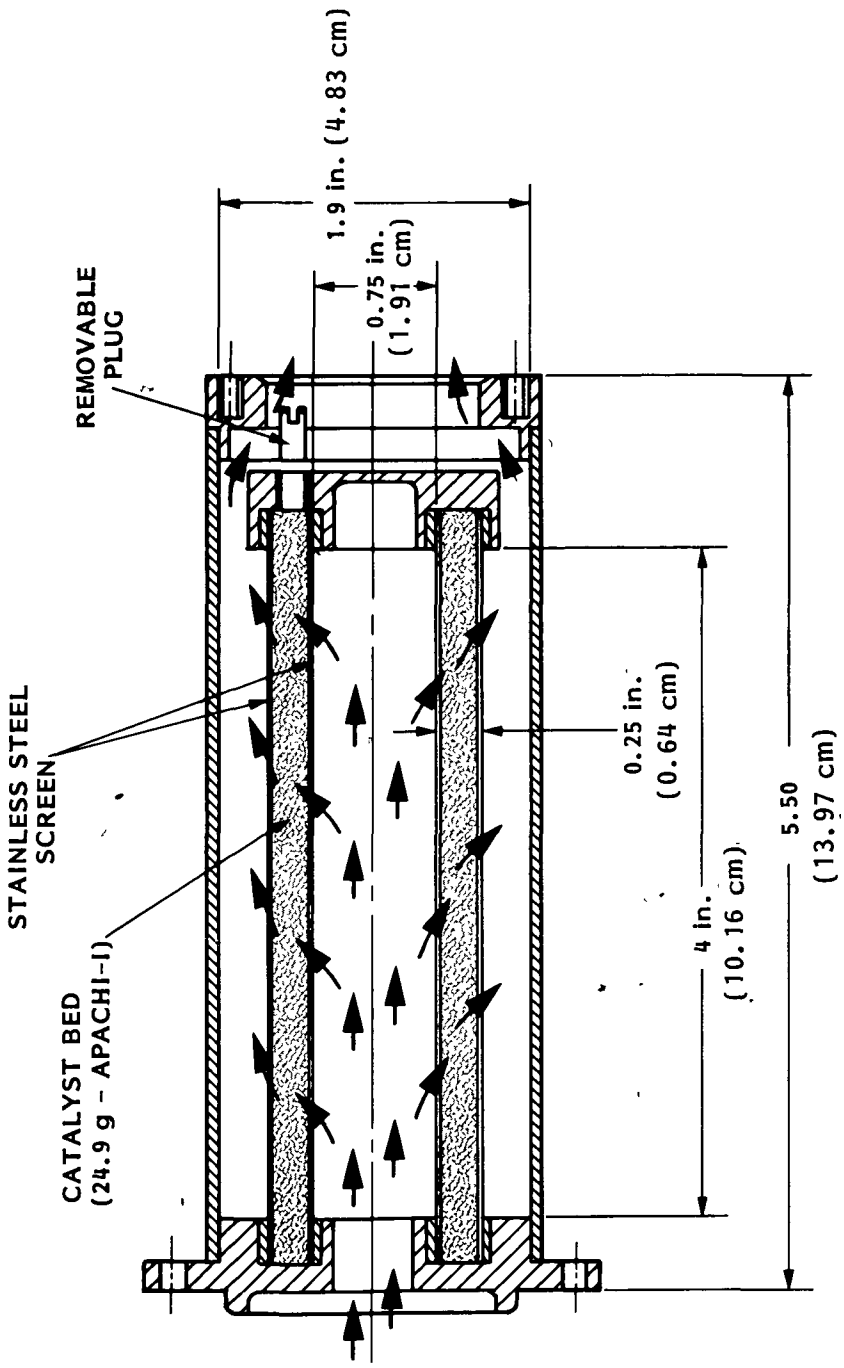

Fig. 2-11 Selected Converter Design

Section 3
TESTING

3.1 TEST APPARATUS

The tests utilized a solid cryogen cooler from a prior program. The cooler was loaded with solid hydrogen and utilized as a low-pressure gas source to the reactor. Details of this cooler and the solid hydrogen tests conducted with it are given in Ref. 13. The cooler's configuration is shown in Fig. 3-1.

The overall test schematic of the system is presented in Fig. 3-2. Details of the reactor setup and the gas analyzer will follow. The test setup provides for evacuation of the insulation space around the hydrogen tank to a vacuum level of 10^{-6} or lower, transfer lines to fill the tank with liquid hydrogen, and a coolant loop which may be utilized to freeze and subcool the liquid hydrogen with helium. The liquid hydrogen may also be solidified by direct vacuum pumping of the ullage space. The reactor is located in the vent line of the cooler. The hydrogen tank can be utilized as a source of gas to the reactor at pressures from approximately 1.38×10^5 Pa down to 1 torr by varying the valve settings, primarily valve V1 to the mechanical pump and valve V4 to the facility vent.

The catalytic reactor assembly consists of the reactor described in section 2.4 along with a LN_2 guard pot and an intermediate shroud with heater to maintain nearly adiabatic conditions for the reactor. The inlet and outlet pressure of the reactor was measured with a Wallace and Tiernen gage with a 0 to 20 torr range. A pair of thermocouple rakes containing 4 absolute and 5 differential thermocouples were mounted on the reactor and can be seen in Fig. 2-12. The cross section of the reactor assembly can be seen in Fig. 3-3. The photograph of the reactor assembly is shown in Fig. 3-4.

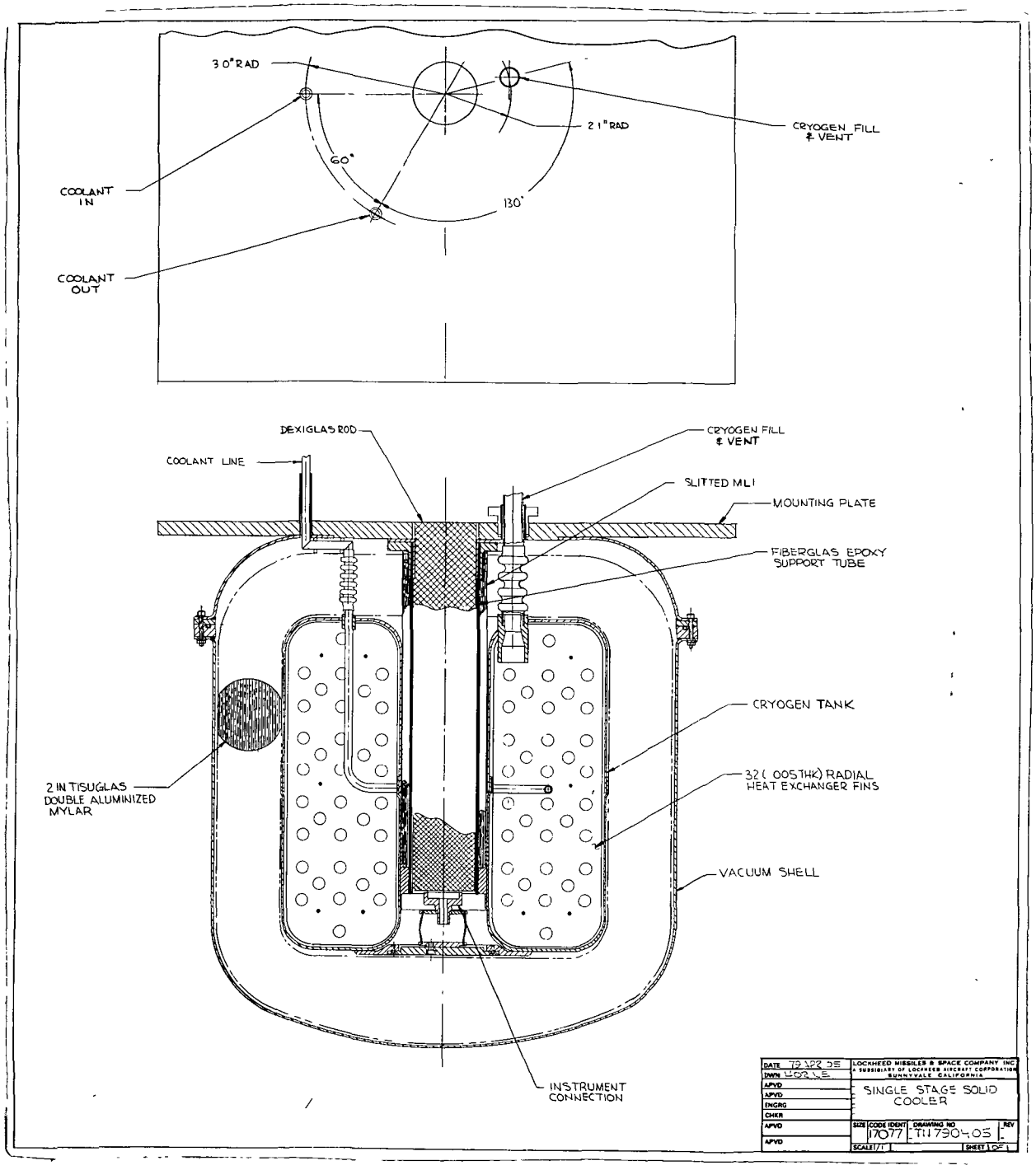

Fig. 3-1 Single-Stage Solid Cooler

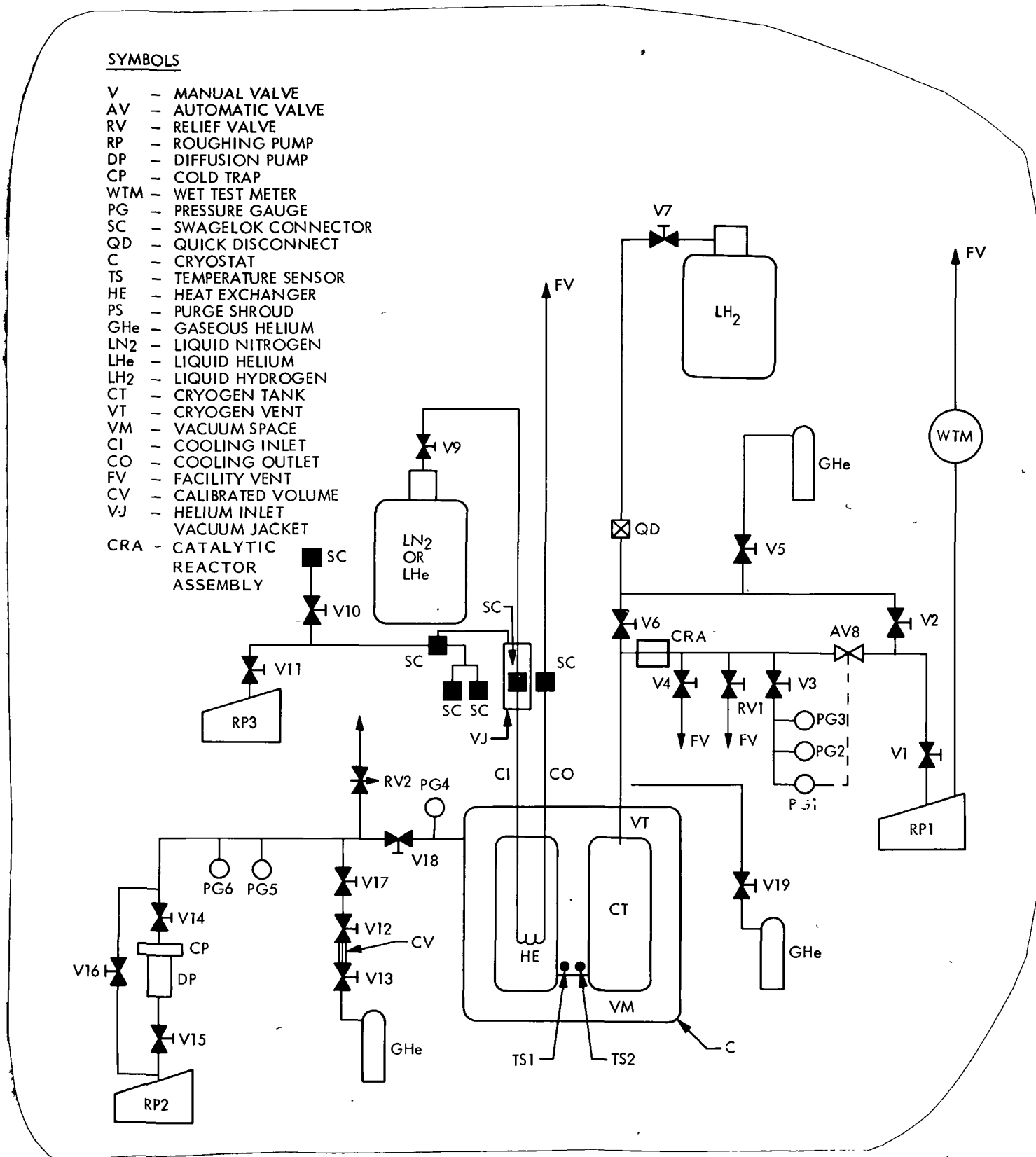

Fig. 3-2 Catalytic Reactor Test Schematic

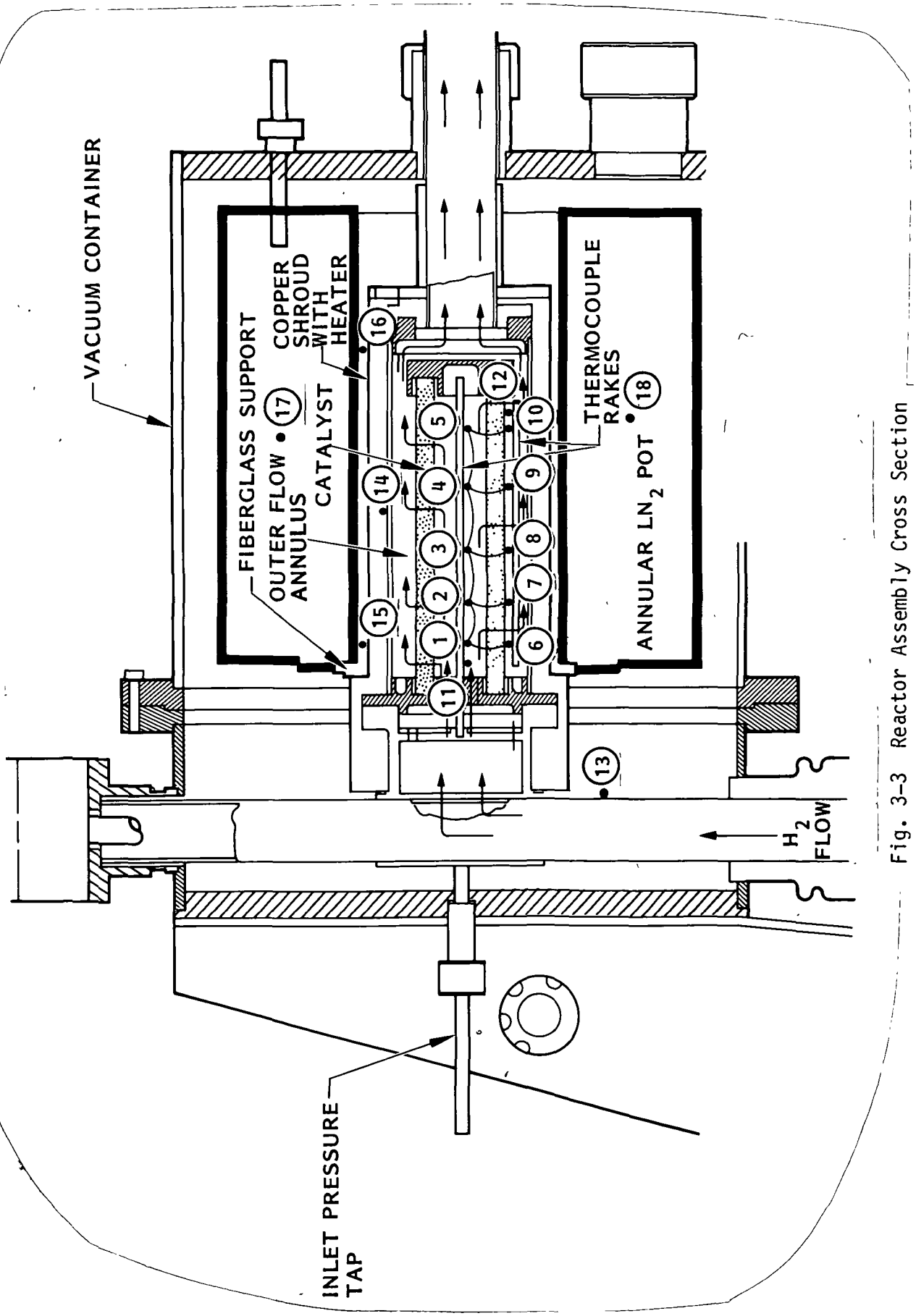

Fig. 3-3 Reactor Assembly Cross Section

During the tests a GOW-MAC Model 24-150 thermal conductivity gas analyzer was utilized. This instrument inferred the para-ortho concentration at the reactor outlet by a measurement of the thermal conductivity of the gas stream.

3.2 TEST RESULTS

Initial tests were conducted without the gas analyzer, relying instead on the temperature measurements in the inlet and outlet streams and performing a heat balance to determine the reactor efficiency. This technique was not successful. Subsequent detailed thermal analysis of the reactor showed that the apparatus was not sufficiently adiabatic for this approach.

The tests with the gas analyzer were conducted in two series: Series I conducted with liquid hydrogen at a pressure of approximately 1.38×10^5 Pa, and Series II with solid hydrogen down to pressures as low as 1 torr.

Series I Tests

The flow diagram for these tests is shown in Fig. 3-5. Numerous combinations of the valves 1-6 can be utilized for calibration of the GOW-MAC to obtain reactor efficiency data and to verify calibration during any point in the test. Initial calibration of the GOW-MAC consisted of passing normal hydrogen gas (25 percent para) through inlet B and boil-off from liquid hydrogen (99.9 percent para) from the test cooler through inlet A.

The flow rates were balanced and controlled by valve adjustments and observations of the flow meters. A second calibration point was obtained by passing the normal hydrogen gas through both sides. In this manner the GOW-MAC was set up to run with normal hydrogen gas as the reference gas for all tests, and the unknown or calibration gas was passed through inlet A. The resulting calibration is shown in Fig. 3-6. Various additional checks on the GOW-MAC operation were also made. For example, LH_2 boil-off was passed through both sides to ensure a zero output of the meter. During the tests the

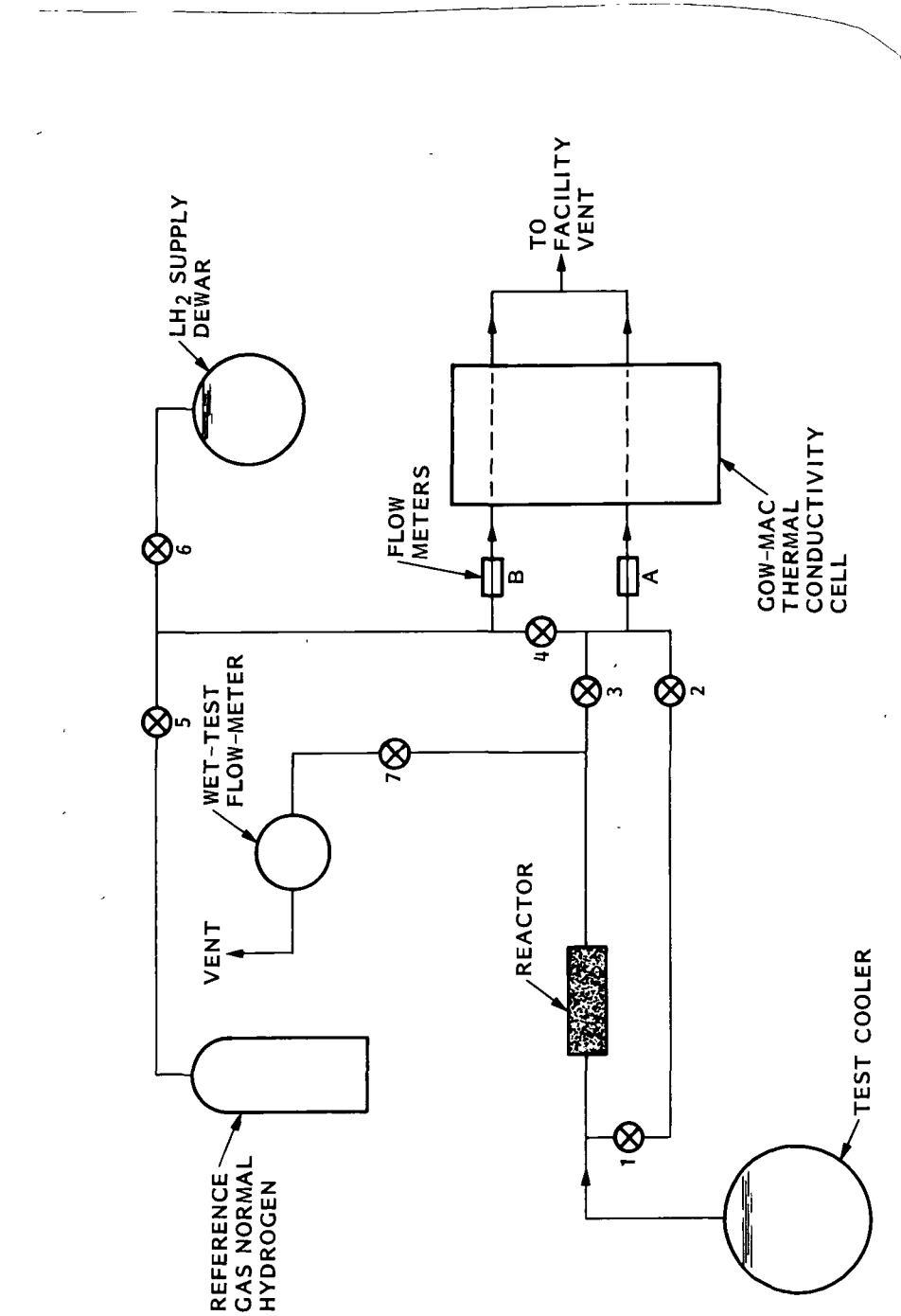

Fig. 3-5 Flow Diagram for Para-Ortho Reactor Tests - Series I

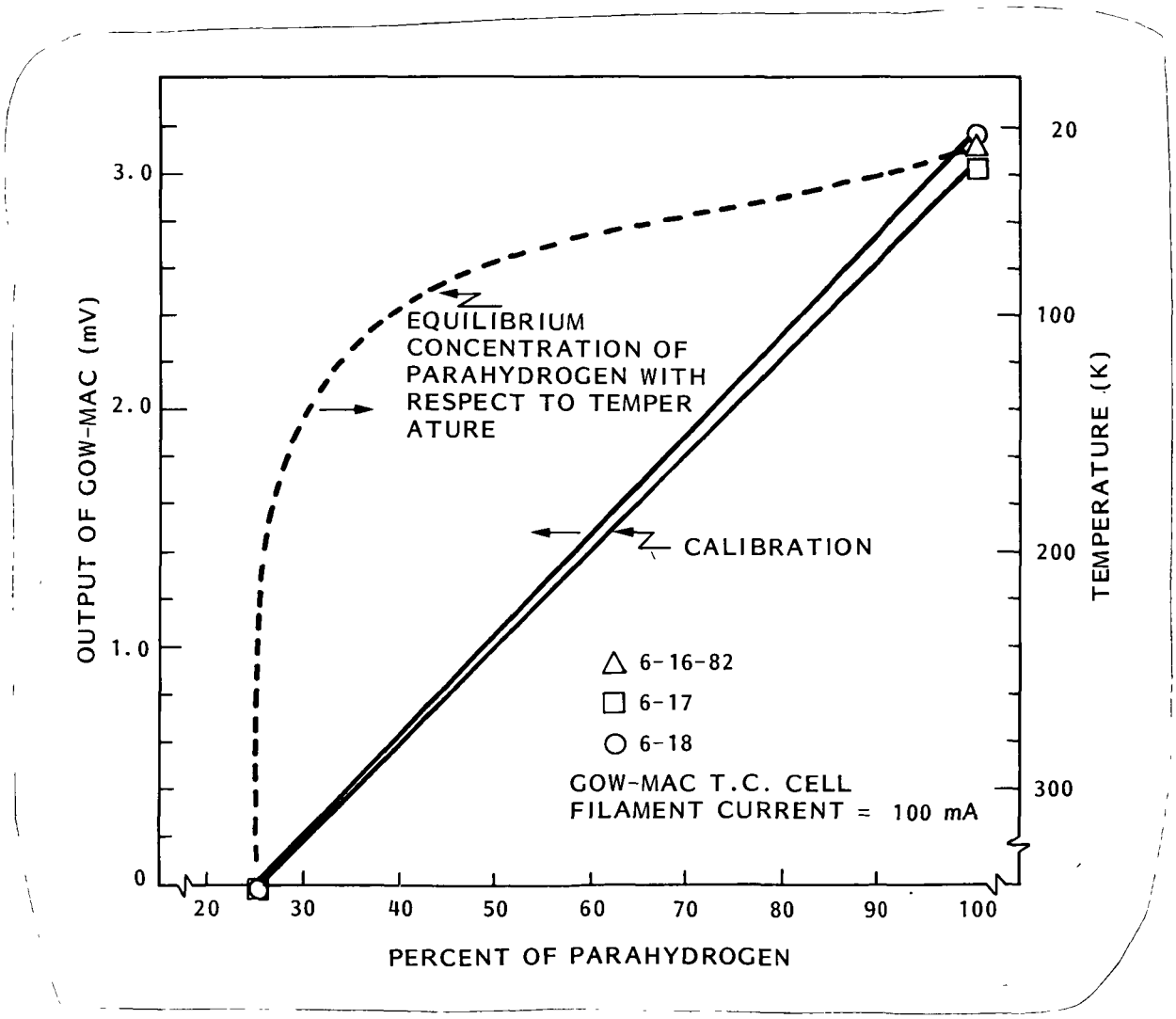

Fig. 3-6 Calibration of GOW-MAC Gas Analyzer

calibrations were checked, for example by opening valve 1 to bring 99.9 percent para to the GOW-MAC to check its output. It was felt that checks of this type were essential to rule out contamination of the gas due to leaks or other sources. The output is very sensitive to minute quantities of foreign gases. During the tests the test cooler was loaded with LH_2 and allowed to self pressurize to approximately 1.38×10^5 Pa and the boil-off gas was passed through the reactor where it was monitored at the GOW-MAC for percent parahydrogen content.

Fig. 3-7 presents the conversion efficiency of the reactor as a function of the volumetric flow rate of H_2. The efficiency is defined as:

$$\text{Percent Efficiency} = \frac{C_{inlet} - C_{outlet}}{C_{inlet} - C_{equilibrium}} \times 100$$

During a test series the reactor temperature tended to change slowly, as it was difficult to establish steady flow and temperature conditions independently. Changes in the flow rate led to changes in reactor temperature. The data were grouped into three temperature regimes shown on the figure. The reaction rate (percent efficiency) is shown to be a strong function of both temperature and flow rate.

The catalyst which was used in the reactor spent a substantial time (several months) exposed to the atmosphere during the various assembly stages and was not heated prior to the tests. Some of the test points were repeated after purging of the catalyst for approximately six hours with room temperature helium. These repeat points showed a negligible effect of this purging as indicated on the figure. Recharging the catalyst with gas at elevated temperatures was not performed.

The data show a strong effect of reactor temperature. The activity at 103-120 K is much higher than at 226-297 K.

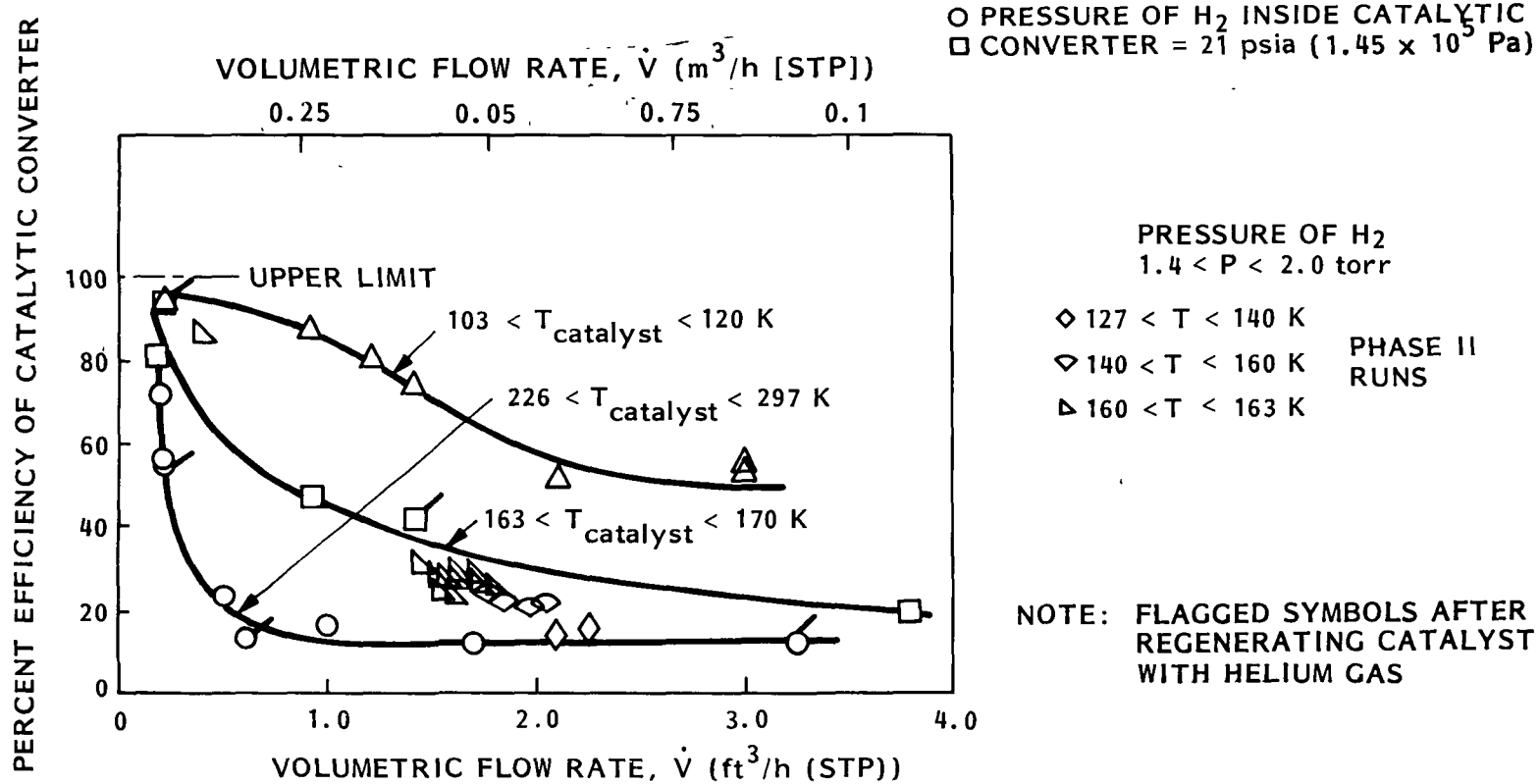

Fig. 3-7 Efficiency of Catalytic Reactor Versus Flow Rate of Hydrogen

Figure 3-8 presents the efficiency of the reactor as a function of the catalyst temperature for various flow rates. The data seem to indicate a maximum reactivity at or near 100 K.

Figure 3-9 presents the percent para-hydrogen at the reactor outlet as a function of the catalyst temperature at various flow rates. The low-pressure data are also shown. The equilibrium concentration of para-hydrogen with temperature is also shown.

During the Series-I tests the pressure drop through the reactor was not measured.

Series II Tests

For the Series II tests the apparatus was modified so that the GOW-MAC apparatus could be calibrated and operated at pressures below atmospheric pressure. The flow diagram for the tests is shown in Fig. 3-10. The calibration of the GOW-MAC was repeated at pressures below 1 atmosphere. Good agreement with the prior calibration was obtained for pressures down to about 1/2 atmosphere absolute. Below this pressure the calibration became unrepeatable and unstable.

During the tests the test cooler was filled with NBP hydrogen and then pumped with vacuum pump A until it was solidified. Once adequate solid hydrogen temperatures were established, the gas sampling proceeded in the following manner: the flow stream from the reactor after passing through the mechanical pump was split into two streams, one going to the flow meter for measurement and the other going to the GOW-MAC. This stream was passed through a LN_2 cold trap to remove contaminants from the pump and then was throttled to a lower pressure prior to passing through the GOW-MAC, where it was metered passing through the GOW-MAC and through a second mechanical pump B, and then to the facility vent. A second LN_2 trap guarded the GOW-MAC from back diffusion of contaminants from this pump. This procedure was necessary to obtain a sufficient pressure head through the GOW-MAC. The pressures in the

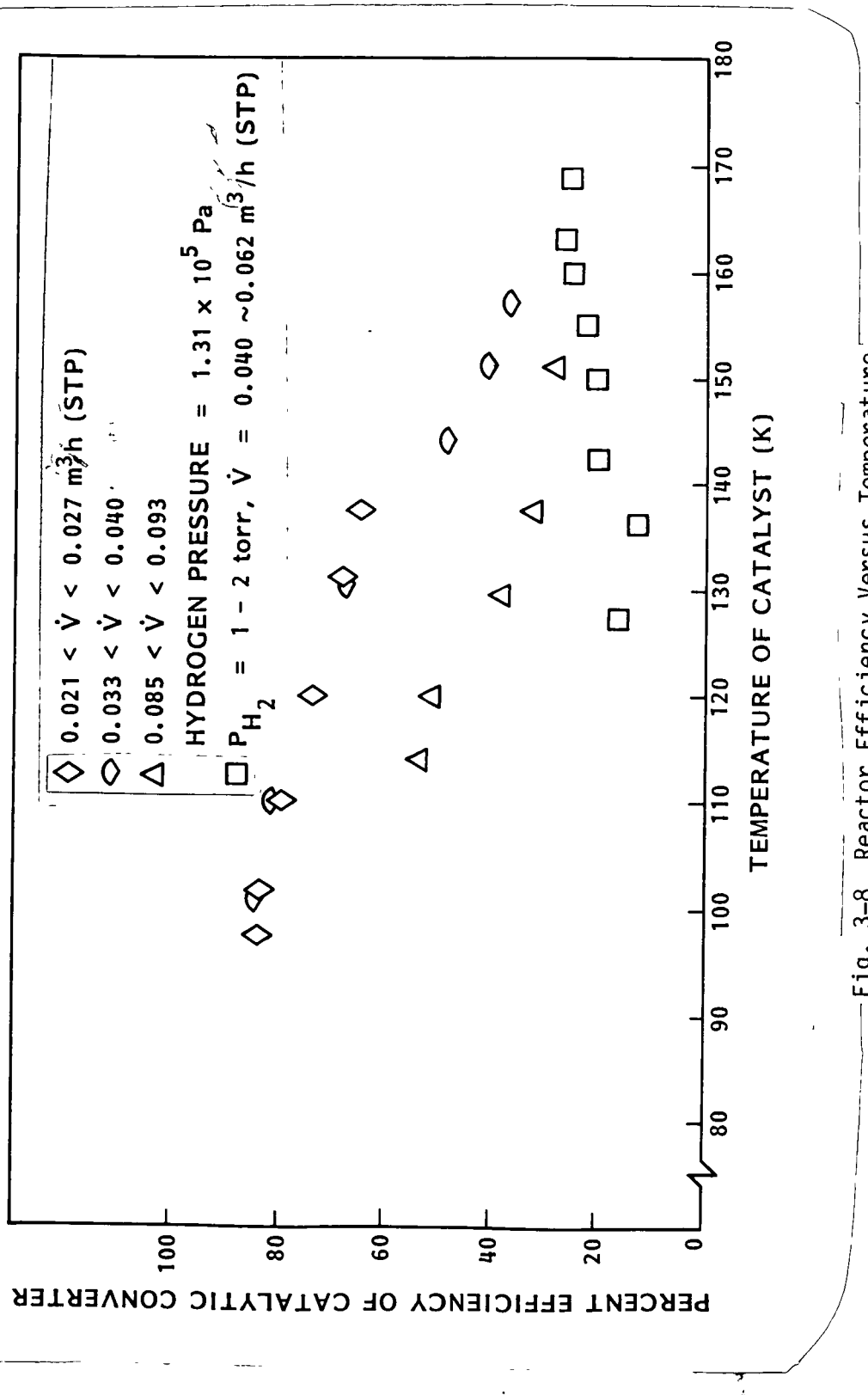

Fig. 3-8 Reactor Efficiency Versus Temperature

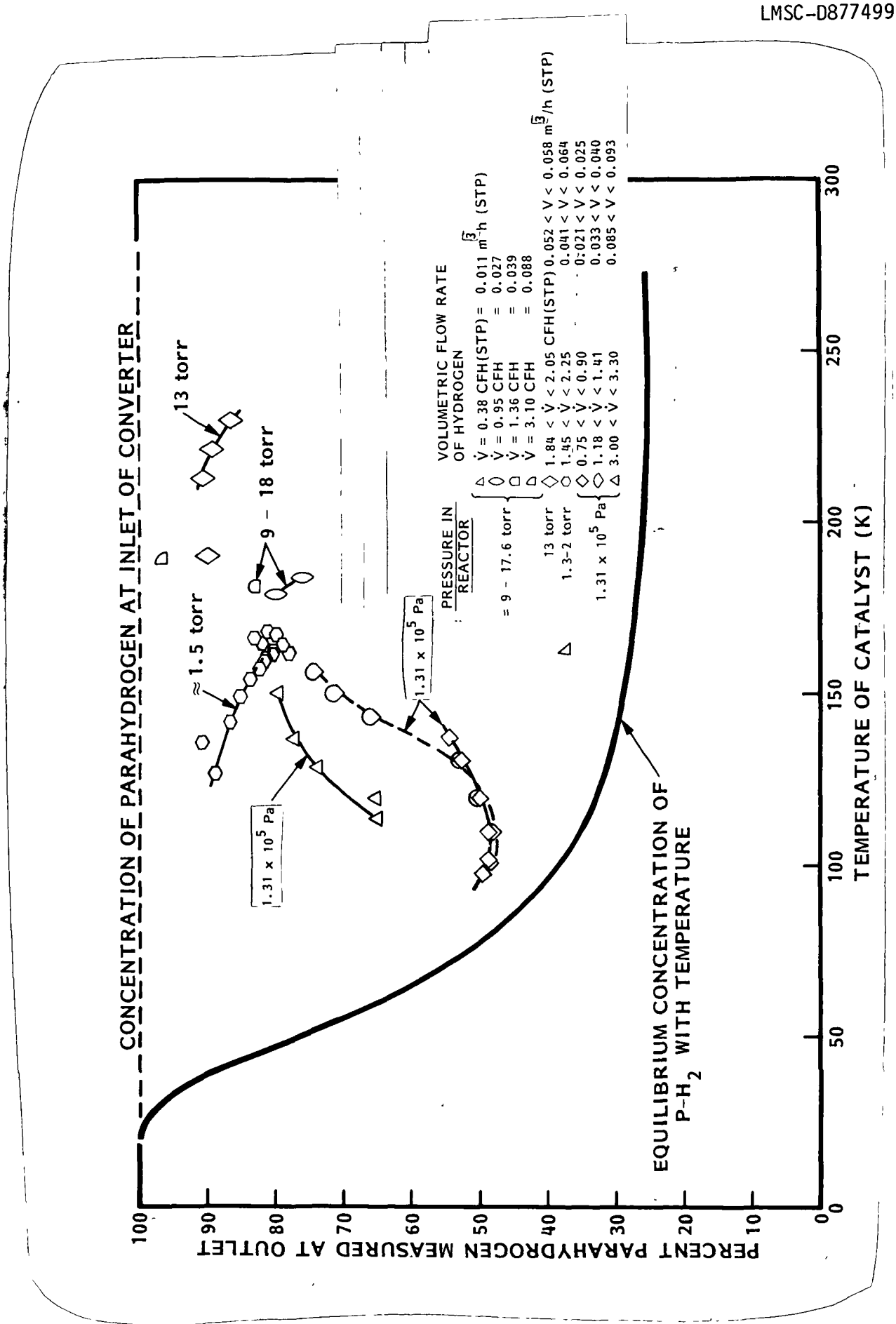

Fig. 3-9 Percent Parahydrogen at Reactor Outlet Versus Catalyst

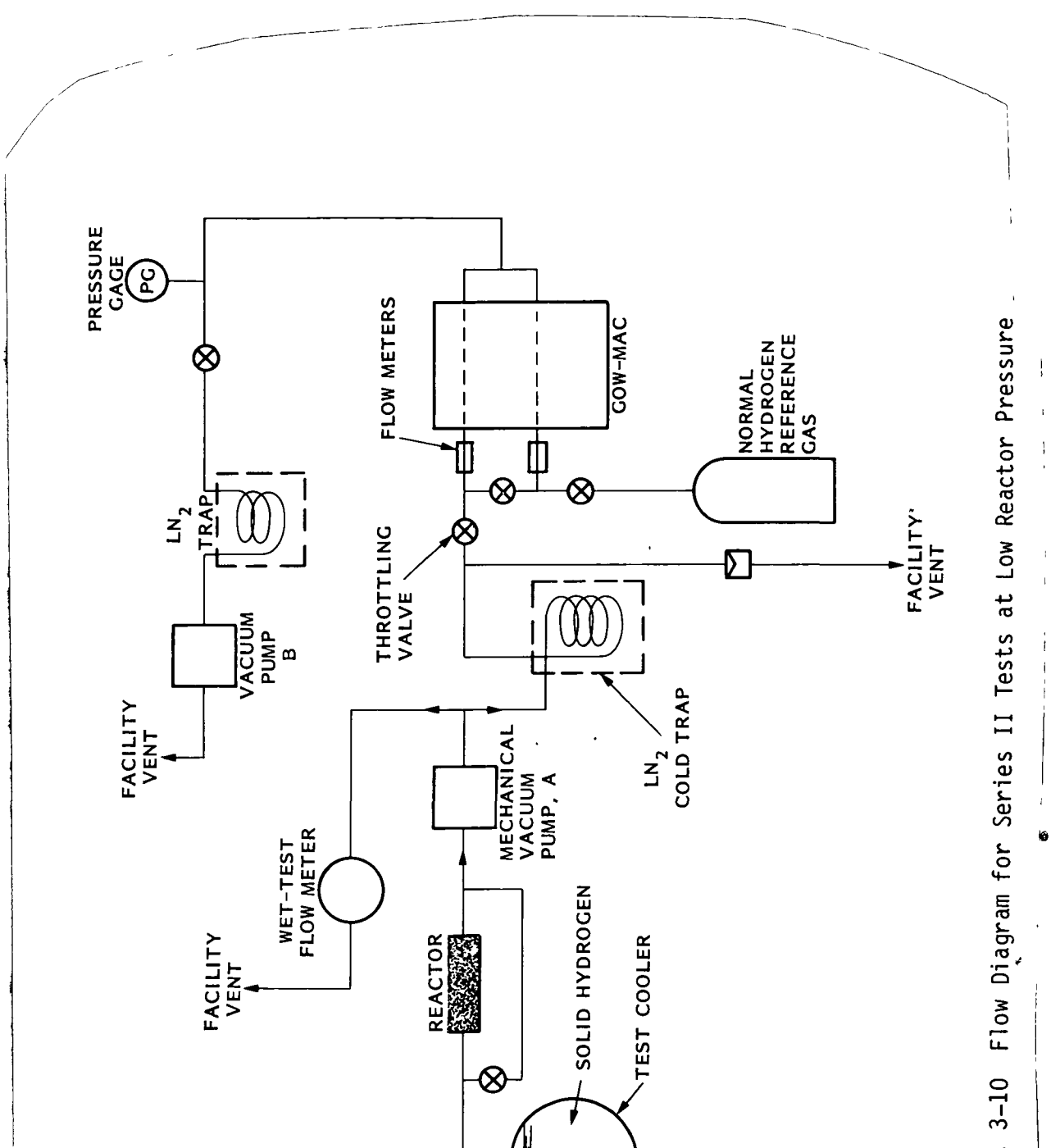

Fig. 3-10 Flow Diagram for Series II Tests at Low Reactor Pressure

GOW-MAC as measured with pressure gage PC were in the range of 5.08 - 10.16 cm of vacuum.

The reactor efficiency data obtained during these tests are presented in Figs. 3-7, 3-8, and 3-9 along with the Series-I data at higher pressures. Figure 3-7 shows the reactor efficiency for tests conducted at 1.4 to 2 torr reactor pressure.

The data are grouped into three temperature ranges. If one compares the data in the 160-163 K range with the data at high pressures (1.45×10^5 Pa), the data appear somewhat lower for the low-pressure runs (27 percent versus 35 percent). The effect of flow rate on efficiency is similar for both pressure ranges.

Figure 3-8 shows efficiency versus catalyst temperature from 127-169 K. The data do not appear to be extensive enough to draw any conclusions about the effect of temperature on reactor efficiency. Because of the reactor operation the lower temperature points are at the highest range of the flow (0.062 m^3/h), and as the temperature increases the flow rates drop to 1.4 CFH at 169 K. Accounting for the flow rate effect on efficiency it appears that there is relatively little effect of temperature on efficiency. One data point is shown at 0.011 m^3/h, 13 torr, and 163 K which indicates approximately 86 percent reactor efficiency, indicating that for sufficiently low flows the efficiency approaches 100 percent.

The low-pressure data for various conditions are also presented in Fig. 3-9 .

Pressure Drop

The pressure drop across the reactor bed was measured with a Wallace-Tiernan gage with 0 to 20-torr range. A correlation between measured and predicted pressure drop is shown in Fig. 3-11. The predicted pressure drop is shown in Fig. 3-11. The predicted pressure drop was based on the Ergun expression (page 2-15). The fractional void volume in the bed was assumed equal to

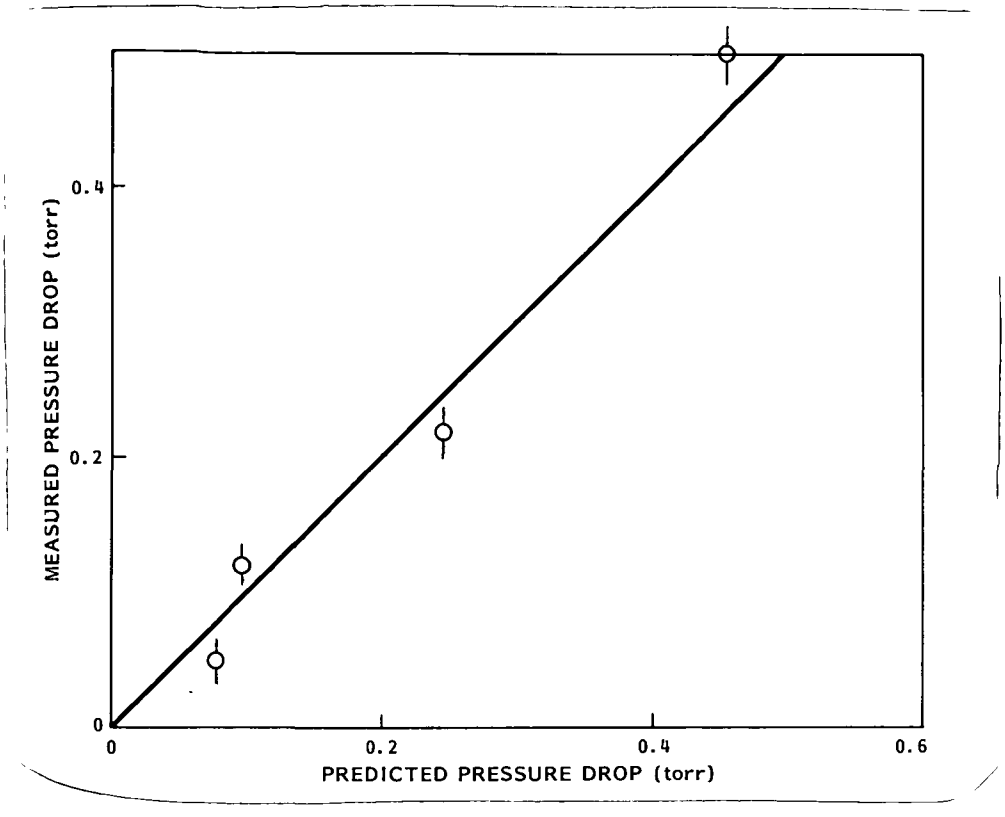

Fig. 3-11 Correlation of Pressure Drop Through Bed

0.45. The particle diameter for the catalyst was assumed equal to 0.0594 cm. This value was selected based upon the 30 x 50-mesh size particles. A 40-mesh average was assumed. The estimated reading uncertainty of the gage is indicated on the data points. The agreement is quite good and indicates the small pressure drops achieved through the bed. The test conditions for this data are summarized in Table 3-1.

Table 3-1 REACTOR PRESSURE-DROP DATA

Flow Rate (m^3/h) (STP)	Reactor Temperature (K)	Average Reactor Pressure (torr)	Pressure Drop (torr)
0.074	85	2.47	0.05
0.058	101	2.06	0.12
0.052	142	1.79	0.22
0.263	167	7.65	0.50

Section 4
CONCLUSIONS

The operating feasibility of placing a catalytic reactor in the vent line of a solid H_2 cooler (or liquid H_2 cooler) has been demonstrated in this contract. The measured pressure drop is quite low and agrees with predictions.

The measured reactor efficiency varied from 10 to 100 percent for the flow rate range of this study. Comparisons with other investigators' data at one atmosphere indicate lower efficiencies for this investigation. One possible explanation of this difference may be the lack of elevated temperature regeneration of the catalyst in this study.

Additional testing is needed to determine the requirements and sensitivity of regeneration at elevated temperatures and to determine the effects of exposure to various environments. The exposure effects and regeneration requirements (if any) must be shown to be compatible with spacecraft ground operations. In particular, the means and limitations on high-temperature regeneration while mounted to an instrument component should be explored.

REFERENCES

1 LMSC-D085818. CLIR Cooler Components Definition Study (Nov. 30, 1979).

2 LMSC-D811574. Upper Atmospheric Research Satellite Cryogenic Limb Array Etalon Spectrometer (CLAES) (July 1981).

3 Scott, R. B., Cryogenic Engineering, D. Van Nostrand Co., Inc., Princeton (1959), p. 289.

4 Bonhoeffer, K. R., and Farkas, A., Trans. Faraday Soc., 28, 242 (1932).

5 Rudham, R., Tullett, A. D., and Wagstaff, K. P., J. Catalysis, 38, 488-90 (June 1975).

6 Brown, D. E., Eley, D. D., and Rudham, R., J. Catalysis, 16, No. 3, 292-302 (1970).

7 Kubicka, H., J. Catalysis, 20, No. 2, 163-71 (Feb. 1971).

8 Eley, D. D., Forrest, H., and Rudham, R., J. Catalysis, 34, 35-40 (1974).

9 Frackiewicz, A., J. Catalysis, 40, No. 2, 184-9 (Nov. 1975).

10 Eley, D. D., and Shooter, D., J. Catalysis, 2, 259-73 (1963).

11 Weitzel, D. H., Draper, J. W., et al., Advances in Cryogenic Engineering, Vol. 2, 12-18 (1956).

12 Singleton, A. H., Lapin, A., and Wenzel, L. A., Advances in Cryogenic Engineering, Vol. 13, 409-27 (1967).

13 Nast, T. C., Study of a Solid Hydrogen Cooler for Spacecraft Instruments and Sensors - Final Report, LMSC-D766177 (Aug. 1980).